JGR Oceans

RESEARCH ARTICLE
10.1029/2022JC018496

The Effect of Harbor Developments on Future High-Tide Flooding in Miami, Florida

F. De Leo[1,2], S. A. Talke[1], P. M. Orton[3], and T. Wahl[4]

[1]Civil and Environmental Engineering Department, California Polytechnic State University, San Luis Obispo, CA, USA, [2]Department of Civil, Chemical and Environmental Engineering, University of Genoa, Genoa, Italy, [3]Stevens Institute of Technology, Hoboken, NJ, USA, [4]Department of Civil, Environmental, and Construction Engineering, National Center for Integrated Coastal Research, University of Central Florida, Orlando, FL, USA

Key Points:

- Tidal range in the Miami downtown area almost doubled over the past century due to human-induced bathymetric change and wetland reclamation
- Pre-1900 tidal predictions are estimated from historical tidal range using a tidal-constituent inference based method
- Increased tidal range increases the probability of high-tide flooding and shortens the time to when sea-level rise will cause chronic flooding

Supporting Information:

Supporting Information may be found in the online version of this article.

Correspondence to:

F. De Leo,
francesco.deleo@edu.unige.it

Citation:

De Leo, F., Talke, S. A., Orton, P. M., & Wahl, T. (2022). The effect of harbor developments on future high-tide flooding in Miami, Florida. *Journal of Geophysical Research: Oceans*, *127*, e2022JC018496. https://doi.org/10.1029/2022JC018496

Received 28 JAN 2022
Accepted 5 JUL 2022

Author Contributions:

Conceptualization: F. De Leo, S. A. Talke, P. M. Orton, T. Wahl
Data curation: F. De Leo
Formal analysis: F. De Leo
Funding acquisition: S. A. Talke, P. M. Orton, T. Wahl
Investigation: F. De Leo, S. A. Talke
Methodology: F. De Leo, S. A. Talke, P. M. Orton, T. Wahl
Project Administration: S. A. Talke
Resources: S. A. Talke
Software: F. De Leo, S. A. Talke
Supervision: S. A. Talke
Validation: F. De Leo

Abstract Little is known about the effect of tidal changes on minor flooding in most lagoonal estuaries, often due to a paucity of historical records that predate landscape changes. In this contribution, we recover and apply archival tidal range data to show that the mean tidal range in Miami, Florida, has almost doubled since 1900, from 0.32 to 0.61 m today. A likely cause is the dredging of a ~15 m deep, 150 m wide harbor entrance channel beginning in the early 20th century, which changed northern Biscayne Bay from a choked inlet system to one with a tidal range close to coastal conditions. To investigate the implications for high-tide flooding, we develop and validate a tidal-inference based methodology that leverages estimates of pre-1900 tidal range to obtain historical tidal predictions and constituents. Next, water level predictions that represent historical and modern water level variations are projected forward in time using different sea level rise scenarios. Results show that the historical increase in tidal range hastened the occurrence of present-day flooding, and that the total integrated number of days with high-tide floods in the 2020–2100 period will be approximately O(10^3) more under present day tides compared to pre-development conditions. These results suggest that tidal change may be a previously under-appreciated factor in the increasing prevalence of high-tide flooding in lagoonal estuaries, and our methods open the door to improving our understanding of other heavily-altered systems.

Plain Language Summary Tabulations of historical tidal range indicate that tidal range in Miami (Florida) has approximately doubled since the 19th century, from 0.32 to 0.61 m. The likely cause appears to be the construction and dredging of the shipping channel to the Port of Miami, though historical land-reclamation may also play a role. In this paper, we show that the increase in tidal range significantly exacerbates the number of minor flood events that are occurring throughout the Biscayne Bay region. As sea-level rise continues, tidal changes will cause high-tide flood impacts to be felt about a decade earlier than would have occurred under historical tidal conditions.

1. Introduction

In the United States (U.S.), the joint impact of sea level rise (SLR) and storm surges may sum up to nearly $ 1 trillion by the end of the 21st century (Neumann et al., 2015). However, there is significant concern that more common, minor flooding may in many locations cause even more damage and disruption, for example, to traffic patterns and travel time (Hauer et al., 2021). Minor flooding is defined as a low level of inundation which induces minor damages to assets and properties, without posing significant threats to public safety (Moftakhari et al., 2018). In previous literature, such flooding events have been also referred to as "nuisance flooding" (Moftakhari et al., 2018; Sweet & Marra, 2015; Sweet & Park, 2014); here, we follow Thompson et al. (2021), and describe these inundation events as high-tide floods (HTF), as they are primarily driven by high-tides. The frequency of these inundation events has increased over the past decades around the U.S. (Moftakhari et al., 2015; Sweet et al., 2018; Taherkhani et al., 2020) and in many locations the future cumulative effects of HTF may outweigh those of the extreme events (Moftakhari et al., 2017). Moreover, locations with changing tidal properties may experience more frequent HTF under future sea-level rise projections, relative to historical norms (Li et al., 2021; Ray & Foster, 2016). Such locations may transition earlier to chronic minor flooding (here defined as ≥100 events per year), compared to stationary tidal conditions.

Tides and tidal datums within many U.S. estuaries and coastal regions are evolving over decadal and secular time scales (Flick et al., 2003; Jay, 2009; Ray, 2009; Woodworth, 2010). Long-term trends in tidal properties

Visualization: F. De Leo
Writing – original draft: F. De Leo, S. A. Talke
Writing – review & editing: S. A. Talke, P. M. Orton, T. Wahl

were detailed, for instance, in the Gulf of Maine (Ray, 2006; Ray & Talke, 2019), along the Columbia River (Helaire et al., 2019; Jay et al., 2011; Talke et al., 2020), within New York Harbor and the Hudson River (Ralston et al., 2019; Talke et al., 2014), in the Delaware Bay (Hall et al., 2013), and in the Saint Johns River, Florida (Talke et al., 2021). Such trends are not explainable by astronomical forcing alone, but are also driven by anthropogenic changes to the geometry of estuaries and harbors (see review by Talke & Jay, 2020), or by changes in inlet geometry (Passeri et al., 2016). Dredging, channel width changes, and other geometric changes were found to double tidal range along parts of the the Cape Fear River (Familkhalili & Talke, 2016), and the Saint Johns River (Talke et al., 2021); Chant et al. (2018) and Ralston et al. (2019) highlighted spatially variable changes in the tidal range in Newark Bay and along the Hudson river, respectively; Lee et al. (2017), Ross et al. (2017), and Du et al. (2018) assessed how SLR and different management scenarios may affect tides in the Chesapeake Bay and Delaware Bay, and Holleman and Stacey (2014) showed how tides might amplify due to increased sea levels in the San Francisco Bay.

While the effects of landscape alterations, dredging and SLR on tides are relatively well researched for river estuaries with major harbors (see e.g., Winterwerp & Wang, 2013), less is known about the historical evolution of tides within back-barrier bays, lagoons, and other semi-enclosed embayments without a significant source of freshwater. A likely reason is that such bays typically did not include major harbors, historically, and therefore were not as likely to have long-term tidal monitoring stations (Talke & Jay, 2013). However, the U.S. Coast Survey (later the U.S. Coast and Geodetic Survey, henceforth referred to as CGS) did make detailed hydrographic maps of all coastal embayments in the 19th and early 20th century. Such hydrographic surveys typically included data from temporary tidal stations, to help with post-processing lead-line measurements of depth. The original records are available in the U.S. National Archives (Talke & Jay, 2013), while the mean tidal range (MTR) and tidal datums from these records are preserved in summary sheets (available from the National Oceanic and Atmospheric Administration (NOAA), henceforth referred to as NOAA; see e.g., Manning, 1988; Talke & Jay, 2017; Talke et al., 2021). Reductions of these records are found in the tide tables published annually for mariners, or in the U.S. Coast Pilot series of publications. Additional records of tidal statistics are often found in the reports of the U.S. Army Corps of Engineers (USACE, Talke et al., 2021).

Evaluating historical changes to the tides and related flood hazard of lagoonal estuaries is particularly important in low-lying, topographically flat regions highly exposed to flood hazards, such as the coastal areas of south-east Florida. These coastal lagoons and back-barrier bays are often highly anthropogenically influenced. Of the 19 coastal inlets maintained by the USACE on the east coast of Florida, 6 were created after 1890 (Dean & O'Brien, 1987). All 19 inlets have been significantly deepened, some by a factor of more than 10. For example, the Point Canaveral inlet is now ∼14 m deep relative to mean lower low water (MLLW), but was first dug in 1951 (Dean & O'Brien, 1987). The Lake Worth Inlet entrance (Port of Palm Beach) was increased from a ∼1 m controlling depth to a ∼11 m, 122 m wide channel, with modifications starting in 1917 (compare the description in USCP, 1900, with NOAA chart 11466-12-2016). The Port Everglades inlet (serving Fort Lauderdale) was first opened by fishermen in 1902, as reported in H.R. (1909) and has been dredged over time to be ∼13 m deep. Finally, the primary channel into Miami harbor was cut across a barrier island beginning in about 1902 (Cantillo et al., 2000), and is now approximately 15 m deep and 150 m wide.

Here, we explore how such large scale changes in inlet geometry can affect lagoonal tides and minor flood hazard, using northern Biscayne Bay as an example. The city of Miami, located on the northwestern side of the bay (Figure 2), is particularly prone to being flooded, with 90% of the municipality less than 6 m above mean sea level (MSL) (Weiss et al., 2011). SLR rates are accelerating (Domingues et al., 2018; Valle-Levinson et al., 2017), and this contributes to the increasing number of floods in the area (Wdowinski et al., 2016). Miami is already experiencing frequent tidal flooding (Hauer et al., 2021), and is also characterized by local subsidence that contributes to increased flooding hazard (Fiaschi & Wdowinski, 2020). Miami is densely populated and valuable assets are present in its coastal area (McAlpine & Porter, 2018; Molinaroli et al., 2019). For all these reasons, the characterization of the flood risk there is of primary interest. However, no long-term, continuous digital tidal records are available for Miami and the wider Biscayne Bay from before ∼2000 and ∼1970, respectively. Hence, characterizing the influence of land-use and channel dredging on system properties and HTF is challenging, because the largest changes occurred in the first part of the 20th century.

In this contribution, we explore how sparse historical measurements can provide insights into evolving tidal properties and HTF hazard. To evaluate how changing tidal properties altered HTF hazard in Miami, we develop and

validate an "inference method," in which a suite of tidal constituents are inferred based on knowledge of historical tidal range and modern constituent values and ratios. We next explore whether our method can be used to assess how HTF are affected by changes to tides in locations where historical time-series are unavailable, circumventing the lack of daily water level records in the area back to the late 19th/early 20th century. We address the following questions: how do historical changes in tidal range due to early 20th century bathymetry modification influence high tide flood frequencies?

2. Data and Methods

2.1. Computation of M_2

In tidal harmonic analysis, the inference method has long been used to estimate constituent amplitudes for conditions in which the available data is not long enough to adequately separate or assess all needed values (Foreman, 1979). The method relies on the known ratios of constituents from astronomic forcing (Cartwright & Tayler, 1971). Since actual tidal constituent ratios vary in coastal and estuarine conditions (Parker, 2007), one can also use observations to constrain the inference. A variation on the inference method was developed and long-used by the CGS to estimate MTR at a station, using only a handful of available tidal constituents (M_2, S_2, K_1, O_1, M_4, and M_6). The method accounts for additional constituents by dividing the forcing into different clusters, and then scaling the effect of small constituents on tidal range through an assessment of their relative astronomical forcing compared to the dominant constituent in the cluster. The equation presented in CGS (1952) reads:

$$MTR = f_f \times \left[\chi_{M_2} M_2 + \chi_{M_4} M_4 + \chi_{M_6} M_6\right], \tag{1}$$

where f_f is an empirical fudge factor equal to 1.02; M_2, M_4, and M_6 denote the amplitude of M_2 and the overtides, respectively; and χ_{M_2}, χ_{M_4}, and χ_{M_6} are defined as:

$$\begin{aligned} \chi_{M_2} &= \cos(v) + \cos(w) + 0.02 + 0.577\left(\frac{S_2}{M_2}\right)^2 + 0.072\left(\frac{K_1 + O_1}{M_2}\right)^2 \\ \chi_{M_4} &= \cos(P_4 - 2v) - \cos(P_4 - 2w) \\ \chi_{M_6} &= \cos(P_6 - 3v) - \cos(P_6 - 3w), \end{aligned} \tag{2}$$

where P_4 and P_6 are the relative phases of M_2 and its overtides, and are expressed as $2M_2{}^\circ - M_4{}^\circ$ and $3M_2{}^\circ - M_6{}^\circ$, respectively. The superscript $^\circ$ indicates the phase of the tidal constituent. The factor of 0.02 in χ_{M_2} includes the effect of N_2 and minor constituents within the lunar semi-diurnal forcing cluster. Similarly, the scaling values 0.577 and 0.072 include the effect of minor constituents such as K_2 (semi-diurnal, solar band) and P_1 (diurnal band). The phases v and w are computed as follows:

$$\begin{aligned} \tan(v) &= \frac{2M_4\sin(P_4) + 3M_6\sin(P_6)}{M_2 + 4M_4\cos(P_4) + 9M_6\cos(P_6)} \\ \tan(w) &= \frac{-2M_4\sin(P_4) + 3M_6\sin(P_6)}{M_2 - 4M_4\cos(P_4) + 9M_6\cos(P_6)} \end{aligned} \tag{3}$$

According to Equations 1–3, the amplitudes of the principal tidal constituents (S_2, M_2, K_1, and O_1), and the phases of M_2 and its overtides suffice to compute MTR at locations characterized by semi-diurnal regimes. In this contribution, we reverse the calculation and explore whether it is possible to estimate major constituents such as M_2, given only the tidal range and a knowledge of the modern constituent ratios. This is motivated by a widespread availability of historical MTR estimates at locations where no long term historical records are available, making standard harmonic analysis impossible.

Because overtide ratios, relative phases, and constituent ratios may change over time, some allowance for their possible effects on tabulated tidal range within Equations 1–3 is needed. To this end, we first assess the typical percentages by which constituent ratios and overtides change over secular time series, using long tide-records from the NOAA at 12 sites characterized by semi-diurnal regimes on the U.S. East Coast (https://tidesandcurrents.noaa.gov, see Figure S1 in Supporting Information S1 for the geographic location of the sites and Figure 1 for the available time-series). At each site we applied harmonic analysis annually to hourly measurements with at least 75% completeness, following Woodworth (2010), after pre-filtering the hourly data using a 2-day Lanczos

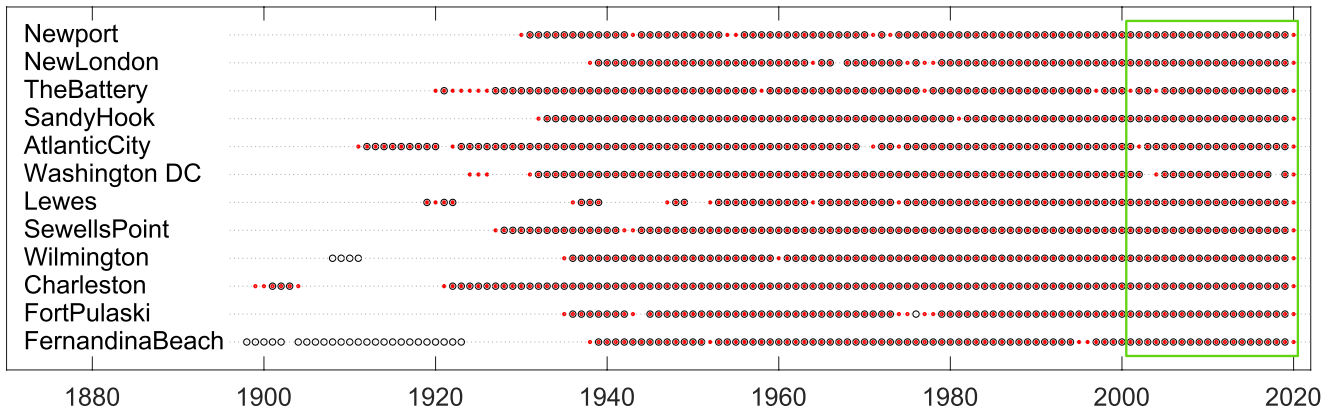

Figure 1. Time-series at the gauges used to validate the inference method. Open markers and red scatters indicate that hourly records and monthly mean high water and mean low water estimates are available, respectively. The green box delimits the modern epoch considered for further analysis. The location and National Oceanic and Atmospheric Administration station numbers of these gauges are shown in Figure S1 in Supporting Information S1.

window to remove most of the non-tidal variability (Ray & Foster, 2016). The harmonic analysis was performed with the U-Tide routine (Codiga, 2011), and carried out on a yearly basis so that standard nodal corrections for the constituents could be employed (Foreman & Henry, 1989; Pawlowicz et al., 2002). For each year available, 59 tidal constituents were computed, including M_2, S_2, K_1, O_1, M_4, M_6, and the respective phases. Using these data, we derived the relative phases and the ratios used in Equations 1–3. Next, we computed the total range of variability for each term in Equation 1, and assumed this is symmetrically distributed around the respective mean value; this assumption was proved to hold at most of the test locations. Next, we computed MTR as the difference between tabulated monthly mean high water (MHW) and mean low water (MLW). These estimates were averaged on a yearly basis, and the 18.6 years nodal cycle was removed.

To test our method, yearly series of M_2 were inferred at 12 NOAA sites (Figure 1), using Equations 1–3, given yearly estimates of MTR and plausible values of constituent ratios and other parameters. An ensemble of possible permutations in the relative phases, the overtides, and the constituent ratios were obtained around their mean value, using the empirically defined bounds and variability defined from harmonic analysis (see above). Each parameter was varied one-at-a-time in a sequential manner through its range (effectively assuming a uniform distribution), and Equation 1 was solved each time. The procedure above led to an ensemble of inferred M_2 values for each year of the time-series. These estimates were validated against the values of M_2 computed through the harmonic analysis, assuming that the latter represent the true (i.e., reference) data.

2.2. Validation of High-Tide Flooding Days Estimates

Li et al. (2021) developed a method to assess the role of changing tides in altering HTF frequency at a given location, as follows. First, the predicted tides based on modern data are removed from present-day water levels. The tidal signal is then reintroduced using a tidal prediction obtained with tidal constituents representing historic conditions. This creates a synthetic time series that approximates what water levels would have been, had tides not evolved. The method assumes that changes in the non-tidal residual are small or negligible. Then, HTF events (i.e., events that exceed a minor flood datum) are counted over the modern epoch using both the measured time series and the synthetic time series.

In this contribution, we assess whether an inference-based method based on Equations 1–3 can assess the effect of evolving tidal range on HTF. For validation, the inference-based method was compared against results using the Li et al. (2021) methodology at the 12 sites shown in Figure 1. At each location, the first available year of the series was used to infer the historical tidal conditions, while the 2001–2019 period was defined as the modern epoch (i.e., the green box in Figure 1). Three types of synthetic tide series for the modern epoch were predicted on a yearly basis by:

1. Using the historical constituents computed from the harmonic analysis of hourly data; this approach is the same as Li et al. (2021).

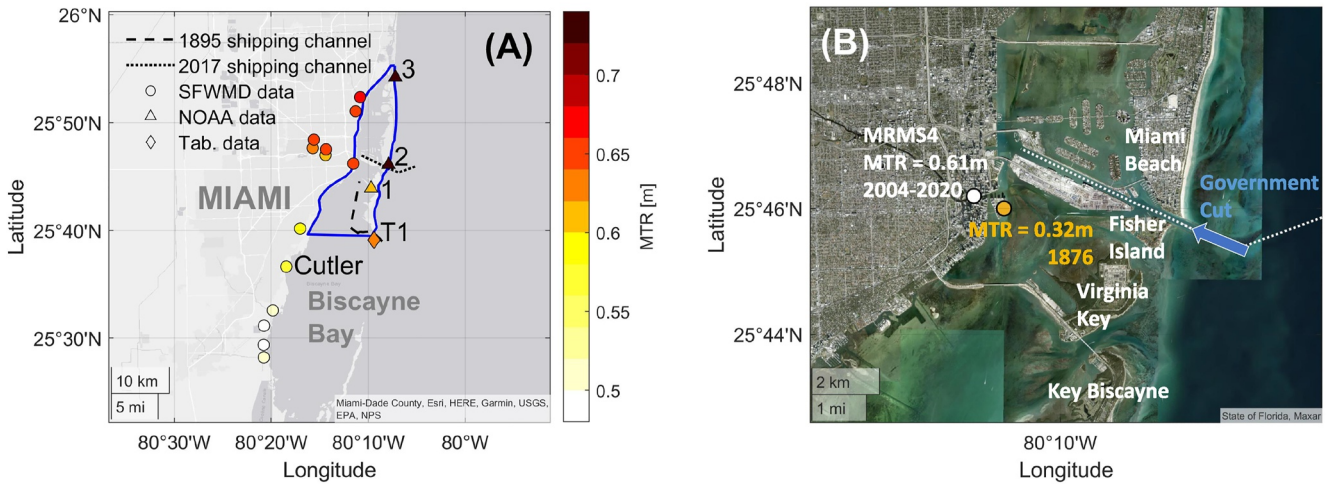

Figure 2. Panel (a): Map of Biscayne Bay and present-day mean tidal range (MTR). The historical shipping channel (dashed line) enters the Bay at Cape Florida (point T1); the modern shipping channel (dotted line) enters near Miami Beach (point 2). Circular markers denote data from the Southwest Florida Management District, triangular markers denote records from long-term National Oceanic and Atmospheric Administration (NOAA) stations, and diamonds denote data from short records tabulated by NOAA. NOAA gauges are numbered as follows: 1 → Virginia Key (station ID: 8723214); 2 → Miami Beach (station ID: 8723170; records available in EV2 database, see Talke et al., 2021, for references); 3 → Haulover Pier (station ID: 8723080). T1 refers to a tabulated MTR estimate from 1981. MTR was computed over 2004–2020, with the exception of the NOAA gauges and T1. The blue line delimits the area used to compute the Choking Number P (Equation 4). Panel (b): close-up on the area of investigation and the gauges used for the analysis of future high-tide floods at Miami (Section 2.3). The years denote the years for which tidal range estimates for downtown Miami were made.

2. Using the modern constituents, but replacing only the M_2 amplitudes with the inferred estimates of historical M_2 (Section 2.1). Three values from the ensemble of M_2 estimates were tested: the bounds of the 95% confidence interval (CI), and the median. This method explores how much HTF change is attributable to M_2 change only.
3. Replacing the amplitudes of M_2, S_2, K_1, O_1, N_2, and the M_4 and M_6 overtides with their inferred historical counterparts, while keeping all other values the same. In this case, the historical amplitude of M_2 was computed as in Equation 2, and was later used to derive the other constituents' amplitude by assuming that the ratios between the latter and the former do not vary and are equal to the mean ratios computed over the modern epoch. Under this assumption, the historical value for a generic tidal constituent A can be simply computed as $M_{2,\text{HIST. EPOCH}} \times \left(\frac{A}{M_2}\right)_{\text{MOD. EPOCH}}$. This will be referred to as "multi-constituent" approach from here on.

HTF days were then computed over the modern epoch according to the three different approaches, and the respective results were compared. HTF days are defined as days where the HTF threshold is exceeded at least once, based on hourly data. Thresholds for minor flooding were defined as in Sweet et al. (2018). Finally, a sensitivity analysis was carried out with respect to the period used to derive the historic tidal constituents, and analysis steps (1–3) were replicated referring to the second and the third year of the series. Using different start years enables us to investigate the effect of random, year-to-year variations in harmonic analysis results, whether caused by data quality (e.g., Zaron & Jay, 2014) or physical processes (Devlin et al., 2014; Moftakhari et al., 2013).

2.3. Computation of High-Tide Flooding Days at Miami

Our tidal inference method was next used to assess how shifting tidal conditions may affect the future occurrence of minor flooding in the downtown area of Miami, in the northern part of Biscayne Bay, South-East Florida (Figure 2).

Pre-1900 tidal constituents in the Miami downtown area were computed through the inference-based method described in Section 2.1, using the historical MTR measured at the mouth of the Miami River (i.e., the brown marker in Figure 2b). This estimate is included in NOAA summary sheets that report Biscayne Bay tidal measurements from 1854 through the 1980s (obtained from NOAA Tides and Currents; see the repository in the Data Availability Statement). The range of possibilities for the overtides and the constituent ratios were based

on the mean values computed from the modern hourly records at gauge MRMS4 from the South Florida Water Management District (SFWMD), which provides the closest modern measurement to the historical location (www.sfwmd.gov; white marker in Figure 2b).

The last year of the available series at gauge MRMS4 (i.e., 2020) was harmonically analyzed to obtain modern tidal constituents. Then, both inferred historical and modern tidal constituents were used to predict tides in the 2020–2100 period; a nodal correction was included, though small in this region (Haigh et al., 2011). Predictions of sea-levels for the 2020–2100 period at Virginia Key were obtained from the Interagency SLR Scenario Tool (https://sealevel.nasa.gov; Sweet et al., 2022), which provides projections through 2150 on a 10-year basis and accounts for vertical land motion. SLR rates for four different scenarios were evaluated: low, intermediate-low, intermediate-high, and high. For each scenario, we applied linear interpolations to derive yearly sea levels starting from the decadal estimates.

Possible future water levels were then estimated for each sea-level scenario for (a) a "tide-only scenario," using tidal oscillation on top of SLR and accounting for the average seasonal cycle of MSL; and (b) a "total water level" (TWL) approach that included SLR, non-tidal fluctuations and seasonal sea level. Seasonal sea-level variability as a function of year-day was obtained by averaging available measurements at gauge MRMS4, after removing tidal fluctuations and applying a 30 days median filter on the detrended yearly residuals. For approach (b), an ensemble driven approach was used to evaluate the possible future evolution of TWLs under different sea-level rise scenarios, using a method similar to Thompson et al. (2021). A total of 15 years of non-tidal residuals were available from the MRMS4 gauge, after accounting for data quality and length. All 15 instances of possible non-tidal residuals over a year were added to each projection of future water levels, which include 4 sea-level rise and the predicted tides using historical and modern constituents (a total of 120 projections; more details are in Sections S2 and S3 in Supporting Information S1). This produced an ensemble of possible TWLs that were then compared to the tide-only cases. Additionally, the analysis of Li et al. (2021) was applied over the 2004–2020 period (see Section 2.2). We use the results to estimate how many additional HTF events have occurred over the last two decades, due to increased tidal amplitudes. Projections were carried out to the year 2100.

Exceedances of the HTF datum were counted for both the 2004–2020 period and the 2020–2100 projection. In the latter case, HTF days were computed for each SLR scenario and both the tide-only and TWL projections. Since no official minor flood datum is available at the investigated location, we derived it through the regression-based approach of Sweet et al. (2018): $y = 0.5 + 1.04GT$, where y is the minor flood (i.e., HTF) datum above the MLLW datum defined for the 1983–2001 epoch, and GT is the great diurnal range (i.e., the difference between mean higher high water (HW) and MLLW). We estimated the MLLW datum for the 1983–2001 epoch using 2004–2020 data, and corrected for SLR between the two periods using known regional SLR. For the sake of brevity, this datum will be referred to as S2018. A recent study of Miami-Dade county by Moore and Obradovich (2020) suggested that minor flooding occurred for water levels that were 20 cm lower than the datum defined by NOAA in the area (see e.g., Sweet & Park, 2014). Therefore, we also evaluate evolving HTF using a datum that is 20 cm below S2018 (the resulting datum will be referred to as M2020 from here on). The S2018 and M2020 datum that we use are 0.63 and 0.43 m above the NAVD-88 datum; by comparison, the NOAA minor flood datum for the Virginia Keys tide gauge is ∼0.58 m above NAVD-88, and the Moore and Obradovich (2020) datum is ∼0.38 m. Therefore, our S2018 and M2020 HTF datums are slightly more conservative (higher) than other thresholds used for high tide flooding, consistent with the slightly larger tides in Miami than at Virginia Key. Details on minor flood datum computation and the areas potentially exposed to HTF can be found in the Supplement (Section S.4, Figures S4 and S5 in Supporting Information S1).

2.4. Biscayne Bay: Water Level Records and Landscape Changes

Gauge MRMS4 belongs to a network of 13 SFWMD gauges that measure water levels along the western side of Biscayne Bay and on the Miami River and its tributary canals. Measurements span the time period 1970–present. Locations of the gauges are shown in Figure 2a (sites highlighted with circles), along with the 3 NOAA gauges available in the area (https://tidesandcurrents.noaa.gov/, sites highlighted with triangles). The NOAA gauges include Virginia Key (station ID: 8723214; time span 1994–2021), Miami Beach (station ID: 8723170; time span 1931–1981), and Haulover Pier (station ID: 8723080; time span 1981–1992). The hourly Miami Beach

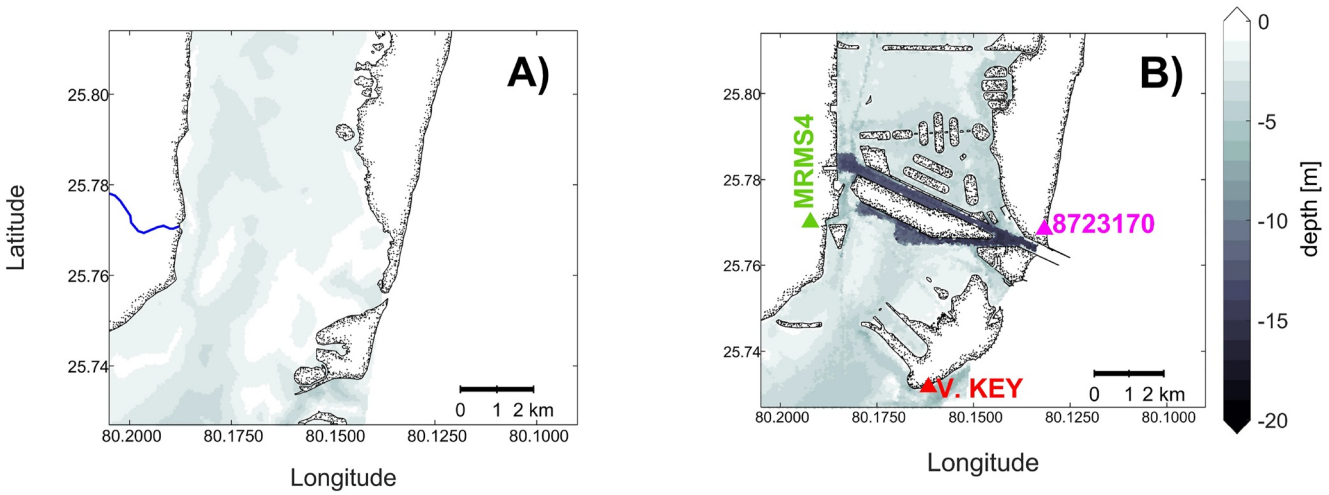

Figure 3. Shorelines in the downtown area of Miami (FL) for different years. Panel (a): 1895; the Miami river is highlighted by a blue solid line; panel (b): 2017; respective charts were digitized through the QGIS software (https://qgis.org). Three tide gauge locations are shown in panel (b), including MRMS4 (green, from South Florida Water Management District), Virginia Key (red, National Oceanic and Atmospheric Administration) and Miami Beach (magenta).

record from 1931 to 1974 was digitized by Talke and Jay (2017) and is available in the GESLA-3 data set (Haigh et al., 2021); additional hourly records are available from 1976 to 1981 from NOAA. Tidal records throughout the Biscayne Bay region were used to detail changes in tides and assess present day conditions.

Biscayne Bay is a shallow, microtidal lagoon with a tidal range that decreases from 0.73 m near Baker's Haulover Inlet (pt 3 in Figure 2a) to approximately 0.5 m in the Southern Bay. The northern part of the Biscayne Bay is approximately 30 km long and from 5 to 9 km wide. Modern bathymetric data from NOAA indicates an average modern depth of 3.2 m with respect to mean sea-level. Freshwater input into the system is minor (the Miami River, Figure 3a, is about 10 km long with a mean discharge of ∼15 m^3/s). To compare the historical and modern coastlines and bathymetry, we first digitized and georectified a CGS chart from 1895 (US Coast Survey chart no. 165), after converting from the presumed chart datum (MLW) to sea-level. Then, we digitized the coastline from NOAA US coast survey chart no. 11468 from 2017. Maps show that, during the past century, extensive land reclamation and navigational development occurred in the area (Figure 3). According to Department of the Interior, U. S. (2002), less than 200 years ago the barrier islands of Virginia Key and Fisher island were attached to Miami Beach (https://npgallery.nps.gov), sheltering what is now the city of Miami from the outer ocean. The Norris Cut inlet (between Fisher Island and Virginia Key, Figure 2b) was formed by a major hurricane (or a series of hurricanes) during the first decades of the 19th century (Department of the Interior, U. S., 2002). The Government Cut was first dredged from 1902 to 1905 to provide direct access to the port of Miami (Cantillo et al., 2000), replacing the old shipping channel that entered the bay south of Key Biscayne (as shown in Figure 2a). Since then, the Government Cut has been periodically dredged and widened during the past century, from a depth of ∼4.6 m and width of ∼18.3 m in 1920 to a depth of ∼15.2 m and a width of ∼152.4 m in 2016. Channel dredging opened the way to the large-scale development of the Miami Harbor, including a number of artificial islands in the inner part of the bay that were built primarily between the 1910s and 1930s (Figure 3b). Based on our evaluation of digitized maps, the surface area covered by water in Northern Biscayne Bay decreased by ∼16.5 km^2 between 1895 and 2017, equal to an approximately 10% reduction in surface area. The analysis of the US Coast Survey maps also reveals that the mean depth in the Northern Biscayne Bay increased from ∼1.7 to ∼3.2 m (see Figure S8 in Supporting Information S1).

Our hypothesis is that the dredging of the Government Cut made tidal exchange between the ocean and Northern Biscayne Bay easier. To investigate whether increased tidal exchange has amplified tides, we computed a composite choking number that includes the effects of multiple inlets in Northern Biscayne Bay for both historical and modern conditions. The inlet choking number captures the reduction in conveyance (i.e., "choking") of

long waves such as tides through an inlet due to geometry constraints at an inlet (Hill, 1994; Stigebrandt, 1980), and is defined as:

$$P = \sqrt{\frac{g A_{cs}^2 H_{cd} T^2}{C_d L \eta A_e^2}} \tag{4}$$

where g is the gravitational force, A_{cs} is the cross-sectional area of the inlet, and H_{cd} and L are the controlling depth and the inlet length, respectively. The drag coefficient is C_d, the surface area of the embayment is A_e, and the tide (long-wave) amplitude and period are η and T. In general, an increase in P indicates a decreasing likelihood that the system is choked. For an idealized, rectilinear inlet, a value of $P \ll 5$ indicates that long-wave amplitudes are damped and significantly reduced within the embayment. When $P \gg 5$, inlet geometry becomes unimportant and tidal amplitudes are unimpeded (Hill, 1994). Because Biscayne Bay is significantly more complex than a one-channel inlet, a simple one-to-one comparison is unlikely to hold. However, if the choking number P has significantly increased in Northern Biscayne Bay, this is consistent with the hypothesis that tides are no longer controlled by choked inlets.

We evaluate a composite choking number for the northern part of the bay (i.e., the blue boundary in Figure 2a), by considering that tidal exchange occurred through 3 channels in the 19th century and occurs today through 5 channels (note that Baker's Haulover inlet and Government Cut were constructed in the 20th century; see Figure 2 for locations). For each inlet, we computed the average cross-sectional area and estimated the controlling depth, for both historical and modern conditions. The computation of cross-sectional areas for the modern inlets used NOAA bathymetry data (see above), while for the historical inlets we used the depths digitized from the CGS map 165 from 1895 (see Figures S6 and S7 in Supporting Information S1 for details on inlet location and computational details). The parameter L was estimated as the length-scale over which the channel was constrained by either levees or by shoals. In both historical and modern cases, we considered η and T equal to 0.34 m and 44700 s, respectively, that is, the modern, coastal M_2 tidal constituent in the area (https://tidesandcurrents.noaa.gov/harcon.html?id=8723214). The drag coefficient C_d was set to 0.0025.

3. Results

Results are organized as follows. Section 3.1 shows the validation of M_2 inferred through Equation 1 against the estimates computed through the harmonic analysis at the locations of Figure 1. The comparison between the HTF events derived from Li et al. (2021) and the inference method is shown in Section 3.2. Section 3.3 reports the analysis of choking number and tidal changes within the bay, while the projection of future HTF according to different SLR scenarios in the city of Miami is shown in Section 3.4.

3.1. Validation of Inferred M_2

Results of the harmonic analysis along the US East Coast reveal that constituent ratios are fairly constant in time, as expected (CGS, 1952). Relative phases and overtide amplitudes are much more variable, consistent with changes in tide propagation and damping caused by anthropogenic modifications (see e.g., Chernetsky et al., 2010; DiLorenzo et al., 1993; Helaire et al., 2019; Ralston et al., 2019; Winterwerp & Wang, 2013). Annual estimates of constituent ratios were found to vary up to ~±15% from the mean values computed over the respective time-series; by contrast, M_4 and M_6 changed by up to 50% with respect to their mean, though much larger percentage changes are possible (Talke et al., 2018). However, even though both changes to the relative phases and amplitudes of the overtides can affect tidal range, in practice the effect is usually small (see e.g., Talke et al., 2018), due to the relatively small amplitudes of overtides in coastal regions (typically <5% of M_2). Based on these results, the allowed percent variability with respect to the mean values was fixed to ±15% and ±50% for constituent ratios and overtides, respectively; relative phases P_4 and P_6 were allowed to vary over the whole 0–2π space, and Equation 1 was solved as explained in Section 2.1.

An example of the time-series of inferred M_2 at Washington DC is shown in Figure 4a, highlighting both the 95% CI of the inferred ensembles (gray lines) and the yearly estimates of M_2 computed through the harmonic analysis (red markers plus 95% CI). M_2 estimates from the harmonic analysis are contained within the inferred distributions for most of the years, indicating overall consistency between the approaches. Because our approach

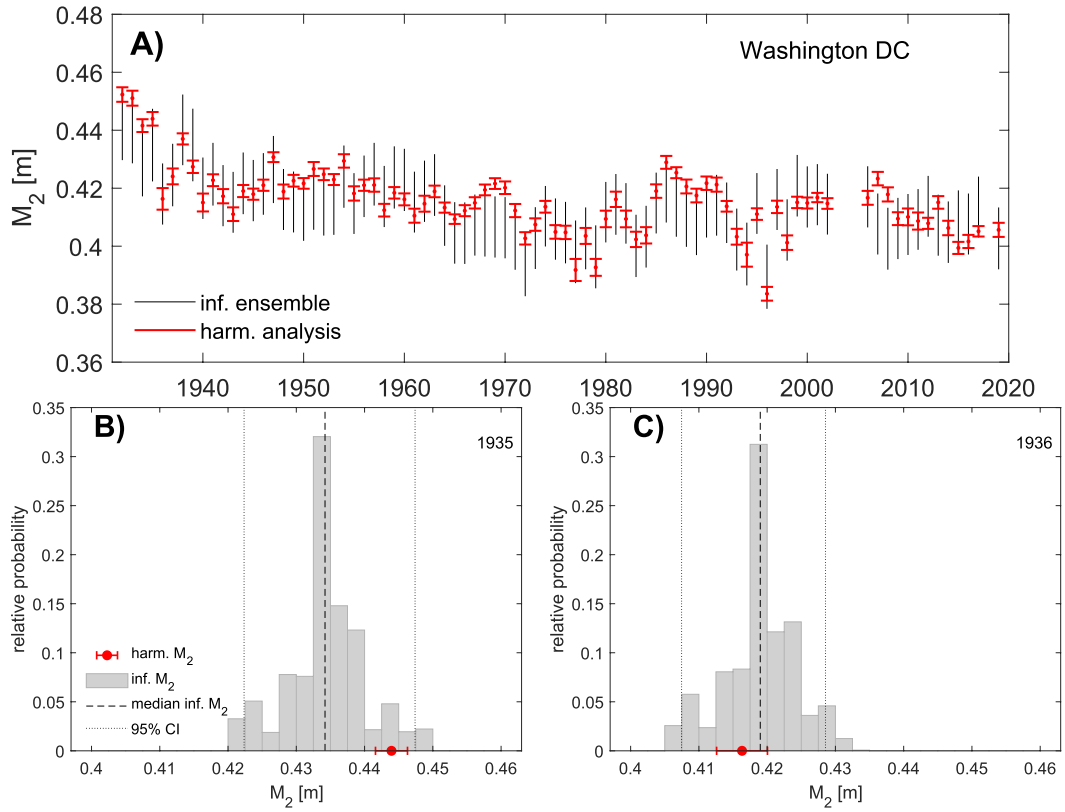

Figure 4. Panel (a): Time series of inferred M_2 at Washington DC. Gray lines denote the 95% confidence intervals (CI) of the yearly inferred ensembles, while the red lines show the 95% CI of the harmonic analysis, being on average ±0.2 cm. Panels (b and c) show the frequency distribution of inferred M_2 and respective median and 95% CI (black dashed line and black dotted lines, respectively) along with the estimates of the harmonic analysis for years 1935 and 1936, respectively.

evaluates an ensemble of possible constituent values, it is not as tightly constrained as constituents from hourly data. The larger spread in our inferred ensemble of estimates is also observed in Figures 4b and 4c, which show the frequency distribution of inferred M_2 from the MTR estimates at Washington DC for two separate years (1935 and 1936, respectively). The comparison shows that the median of the inferred distribution (vertical dashed line) changes due to shifts in the (nodally corrected) MTR. A similar decrease in M_2 from harmonic analysis from 44.4 to 41.6 cm between 1935 and 1936 also occurs. Causes for inter-annual variability can include alteration in dynamical influences such as river flow (e.g., Moftakhari et al., 2013) or gauge timing errors (Zaron & Jay, 2014). Regardless, variations in the calculated and inferred M_2 track each other from year to year for this location, following a general downward trend of ~4–4.5 cm per century (as calculated by Talke & Jay, 2020).

Table 1
Error Metrics Computed Between the Yearly Series of Harmonically Analyzed M_2 and the Median of the Inferred Estimates

Gauge	Bias [cm]	RMSE [cm]	Gauge	Bias [cm]	RMSE [cm]
Fernandina Beach	0.20	0.68	Washington DC	−0.12	0.62
Fort Pulaski	0.29	0.86	Atlantic City	0.37	0.80
Charleston	−0.25	0.85	Sandy Hook	0.46	0.64
Wilmington	2.13	2.57	The Battery	0.13	0.46
Sewells Point	−0.29	0.41	New London	1.64	1.69
Lewes	−0.34	0.58	Newport	0.08	0.51
All Data				0.34	1.06

Next, we assessed the goodness-of-fit between the time-series of annual M_2 computed through the harmonic analysis and the inference method; for the latter, we used the median among the inferred distributions (e.g., the dashed lines in the examples of Figure 4). Results for all the gauges are reported in Table 1 and show that the root mean square error (RMSE) and the bias (i.e., the difference between the mean values of the inferred and harmonically analyzed M_2 series) are <1 cm in 10 out of 12 sites. At Wilmington and New London, RMSE are slightly higher, that is, 2.57 and 1.69 cm, respectively, indicating a 4.4% and 4.7% deviation from the mean values of the harmonically analyzed M_2 series. We conclude that ensembles of inferred M_2 reasonably approximate those from harmonic analysis, but with larger uncertainty. Hence, the constituent inference method is best applied to regions with a large change in tidal range, to ensure a reasonable signal-to-noise ratio. As shown later, the larger uncertainty does not appreciably influence our

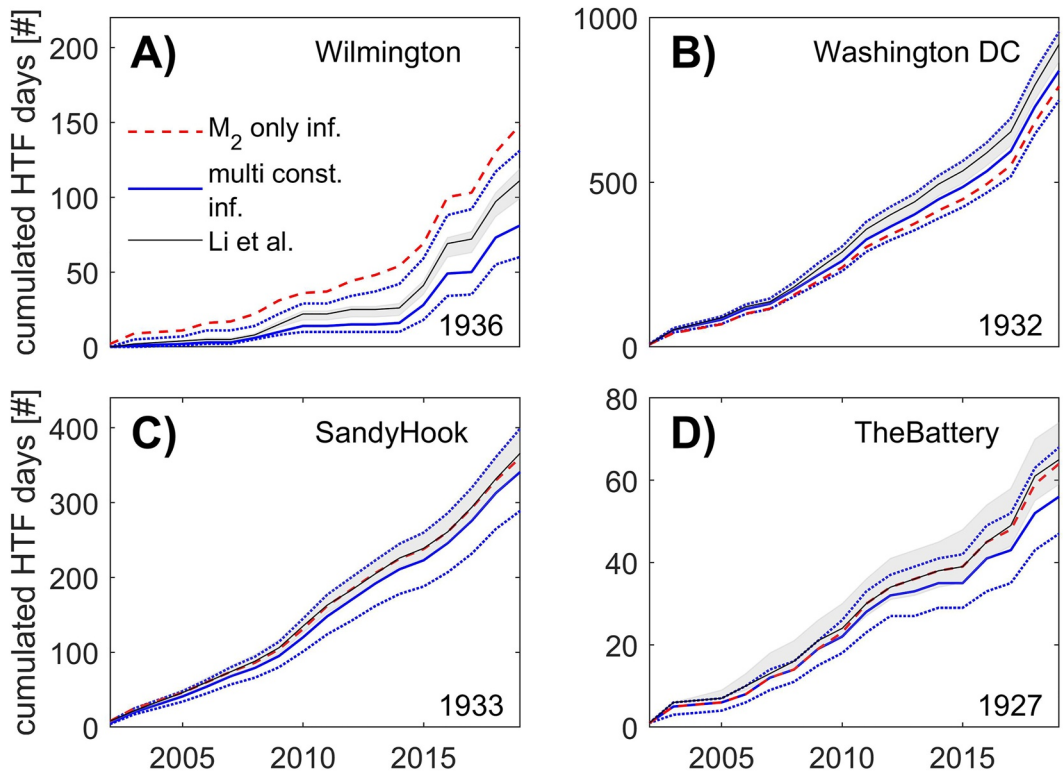

Figure 5. Cumulative high-tide floods days over the 2001–2019 period computed by replacing M_2 only (red curves; results related to the median values of the inferred ensemble) and through the multi-constituent approach (blue solid curves and blue dotted curves for the results related to the median and 95% bounds of the inferred ensemble, respectively). Gray shaded area indicate the bootstrapped 95% confidence bounds of the Li et al. analysis, while black solid curves are related to the expected values of the tidal constituents. Also shown in the lower right corner of each panel is the year retained as historical epoch. Panel (a): Wilmington; panel (b): Washington DC; panel (c): Sandy Hook; panel (d): The Battery.

comparison of HTF under historical and modern conditions at Miami, since the uncertainty is much smaller than the observed change in tidal range.

3.2. Validation of the HTF Estimates

Next, we evaluated whether the inferred M_2's and/or a reduced number of other constituents can determine the number of HTF that would have occurred at our test locations, had tidal constituents remained stationary at historical norms.

Results in Figure 5 show that the cumulative number of HTF days since the year 2000 estimated using our inferred historical constituents (method 2 & 3, Section 2.2) well approximate the Li et al. (2021) method (method 1, Section 2.2). At Washington DC (Figure 5b) and Sandy Hook (Figure 5c), methods 2 and 3 (Section 2.2) obtain similar answers, with the multi-constituent approach (method 3) yielding slightly more and slightly fewer HTF days, respectively. Note that the differences between the M_2 trends at Sandy Hook and The Battery are negligible ($O(10^{-1})$ mm/yr), and little difference is observed in the tides and in their secular change over time (Talke et al., 2014). Therefore, the large differences in the evolution of HTF are primarily attributable to a 0.20 m difference in the HTF datum (panels c and d for Sandy Hook and The Battery, respectively).

In general, the multi-constituent approach adjusts HTF days by $<\pm 0.5\%$ over the 2001–2019 period with respect to the estimates obtained by replacing M_2 only, indicating that changes in the M_2 amplitude dominate changes to HTF. The major exception is Wilmington (panel a): there, the synthetic tidal series computed with the inferred values of M_2, S_2, N_2, O_1, K_1, and the overtides (method 3, Section 2.2) halves the HTF days computed by replacing M_2 only (method 2, Section 2.2). This location is indeed characterized by a large upward trend in MTR (Familkhalili & Talke, 2016; Flick et al., 2003). Because the magnitude of non-M_2 constituents has also

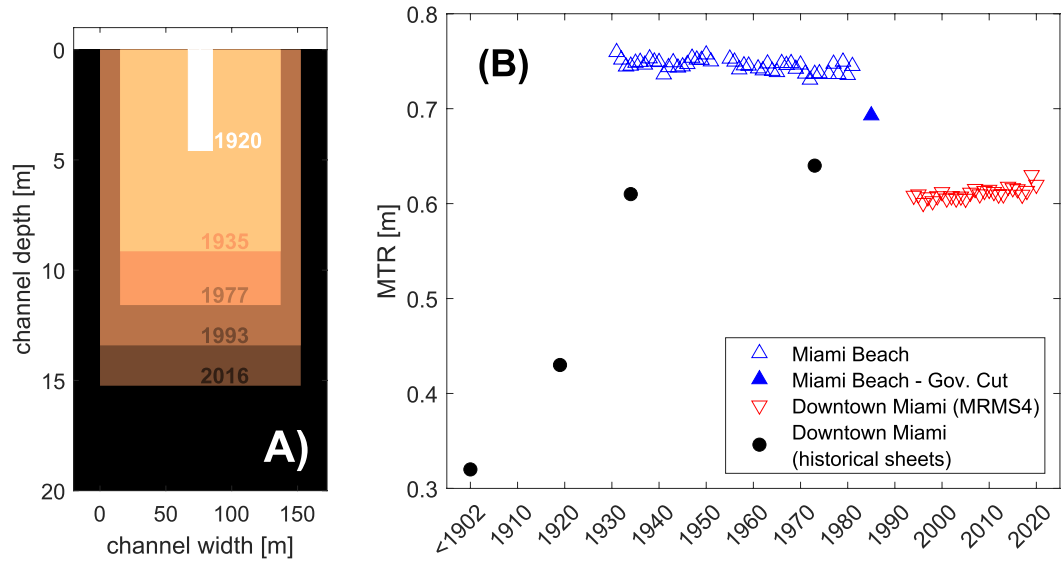

Figure 6. Panel (a): Dredged depths of the Government Cut through the years between 1902 and 2016 (measures from 1920 were retrieved from Cantillo et al. (2000)); panel (b): corresponding tidal changes in the proximity of the Miami downtown area (black markers and red markers for tabulated estimates and MRMS4 data, respectively) and at coastal locations at Miami Beach (highlighted in blue; empty markers refer to station 8723170, filled marker refer to the Government Cut location; see Figures 2b and 3b).

significantly changed, including an estimate of their change evidently alters the number of HTF days. Since the goal of the present work is to characterize the effect of changing tides on HTF at a location that experienced a doubling of MTR (see Section 2.4), the comparison below with the Li et al. (2021) estimates uses the multi-constituent inference approach.

CI of the Li et al. (2021) HTF curves (Figure 5) were computed by bootstrapping the historical tidal constituents using the 95% CI provided by U-Tide, and lie within the boundaries provided by the inference method at Wilmington (panel a), Washington DC (panel b), and Sandy Hook (panel c), while they partially overlap at The Battery (panel d); however, because the CI of all curves overlap, any differences are statistically insignificant and we conclude that estimates from different methods are commensurate with each other. Similar outcomes were found at other test locations and for two different historical epochs. The yearly HTF days related to Li et al. (2021) lie within the inferred HTF bounds in 576 out of 684 total cases (i.e., 3 yearly historical epochs × 19 years of the modern control period × 12 gauges). The inference method either underestimates or overestimates the Li et al. (2021) results by 1 HTF day/year in 72 cases, 2 HTF days/year in 22 cases, 3 HTF days/year in 11 cases, and 4 HTF days/year in 1 case. The largest underestimations are found at Washington DC, where the inferred HTF days are underestimated by 5 days out of 123 HTF days (as provided by the Li et al., 2021, curve), that is, a ∼4% error.

The analysis of the HTF days shows that the inference-based method (Sections 2.1 and 2.2) can be used to make reasonably accurate predictions of historical tides in semidiurnal systems, particularly for conditions in which tidal range has significantly changed and no in-situ measurements of historical tides are available. Therefore, we conclude that our approach can safely be applied to Miami.

3.3. Biscayne Bay: Tidal Changes

Historical summary sheets from NOAA show that 19th century MTR at the mouth of the Miami River was 1.06 ft (∼0.32 m), based on 65 measurements of high and low water from between March and May of 1876. By contrast, the MTR measured by gauge MRMS4 was 0.61 m over the 2004–2020 period. This gauge lies approximately 700 m from the historical measurement; given the closeness of the historical and modern locations, and the lack of significant local gradients in tidal range (Figure 2a), we consider the measurements to be coterminous. Hence, tidal range in Miami has approximately doubled since the 19th century (Figure 6).

The increase in tidal range at Miami appears to have occurred primarily during the first 3 decades of the 20th century, when depths in the Government Cut most prominently changed, from 0 (1902) to ∼9 m (1935; see Figure 6a). Before the Government Cut was first dug, tidal range at Miami was 0.32 m. Tidal range increased to 0.43 m by 1919, based on 3 months of measurements from January–March 1919. Tides continued increasing over time as the channel sequentially became deeper. By 1934–1935, when the shipping channel was ∼9 m deep, tidal range was already reported to be 0.61 m; in 1973, the tidal range reported at the nearby ship base (Gauge 8723155) was 0.64 m, nearly the same as the modern estimate of 0.61 m at station MRMS4. By contrast, hourly Miami Beach records from 1931 to 1974 suggest that coastal tidal constituents and tidal range have not increased from 1931 to the present (Figure 6b).

Available tabulations also suggest that tidal range has also increased throughout Biscayne Bay. At Cape Florida (gauge T1 in Figure 2a), tidal range increased by 0.16 m between the 1850s and 1981, with most of the change (0.12 m) occurring after 1919. The current range at Cape Florida (0.62 m) is similar to Miami, possibly suggesting tidal range at Cape Florida is being influenced by changes in the northern bay. Tidal range has also increased by ∼0.1 m at Cutler since 1919 (see Figure 2 for locations). Moreover, evaluation of tidal records from the SFWMD from the 1980s-present suggests that statistically significant upwards MTR trends are occurring in the southern part of the bay, with trends on the order of 0.4–0.9 mm/yr. The occurrence of large tidal change in northern Biscayne Bay during a period of navigational improvements in the early 20th century suggests that tidal exchange through the Government Cut significantly increased tidal amplitudes (Figure 6). We investigate the correlation between channel deepening and tidal change evident in Miami during the early 20th century by estimating the inlet choking number for northern Biscayne Bay under both historical (1895) and modern (2017) conditions, as described in Section 2.4. Results suggest that the choking number has increased from P ∼3.3 (1895) to P ∼15.3 (2017), a significant increase of more than 4x that is consistent with the bay moving from a choked condition historically to an unimpeded system today.

3.4. Computation of HTF Days at Miami

The doubling of tidal range in Miami since 1900 contributes significantly to present and future HTF hazard in Miami (Figures 7–9). Using the tide-only approach the number of HTF floods begins rising earlier under modern conditions (black curve) compared to historical conditions (blue shaded area), for each SLR scenario (Figure 7). Because historical tides were smaller, the historical scenarios begin exceeding the minor flood datum at a later time (to the right in the panels) compared to the modern-day tidal flooding scenario. However, because there is a smaller spread in the distribution of HW levels in the historical tidal regime, it takes fewer years after flooding onset to reach the saturation value of 365 flood days per year with historical tides, for high and intermediate-high SLR rates. Further, the steepness of the slope (i.e., rate of change in the number of inundation days per year) is larger in the higher SLR scenarios (compare panel c with panel a), but also due to the larger SLR rates in the future (due to acceleration in SLR). For this reason, the slope of the blue curves is usually slightly steeper (at each HTF per year value) than the respective black curve (modern tides) for a given SLR scenario.

The observed effects of SLR on tide-only flooding (Figure 7) is strongly influenced by the seasonal sea-level cycle (Figure 8). As in Figure 7, the transition from the occurrence of the first HTF days to permanent daily flooding (i.e., at least 1 inundation event per day) is shorter for the high SLR scenario (panel a) compared to other scenarios. No permanent flooding is observed for intermediate-low or low SLR for either historical or modern tidal conditions. The observed flooding patterns also show that seasonal sea-level variability drives patterns of tidal flooding in Miami, rather than astronomically driven "king tides" and seasonality in MTR. This is because the seasonal variation in sea-level (∼0.25 m, peaking during fall; see Figure S2 in Supporting Information S1) is much larger than the seasonal excursion in tidal constituents (∼1–2 cm on average) and the difference between mean HW and mean spring tide (∼0.04 m; the latter being computed as $M_2 + S_2$, see Haigh et al., 2011).

A summary of the comparison between HTF days computed from modern and historical tidal conditions is reported in Table 2, showing that amplified tides can account for as much as +>200 HTF days per year by 2100 under high and intermediate SLR scenarios. The largest differences are observed for the intermediate-low SLR scenario (Figures 7c and 8c): in this case, pre-1900 tidal conditions would reduce the total number of HTF by ∼6,000 days spread over approximately 60 years (i.e., 2040–2100, see Table 2). By contrast, the low SLR scenario yields the smallest difference, that is, ∼2000 HTF days spread over a similar period; in this case, historical tidal conditions would result in almost no tide-only flooding, as shown in Figures 7 and 8.

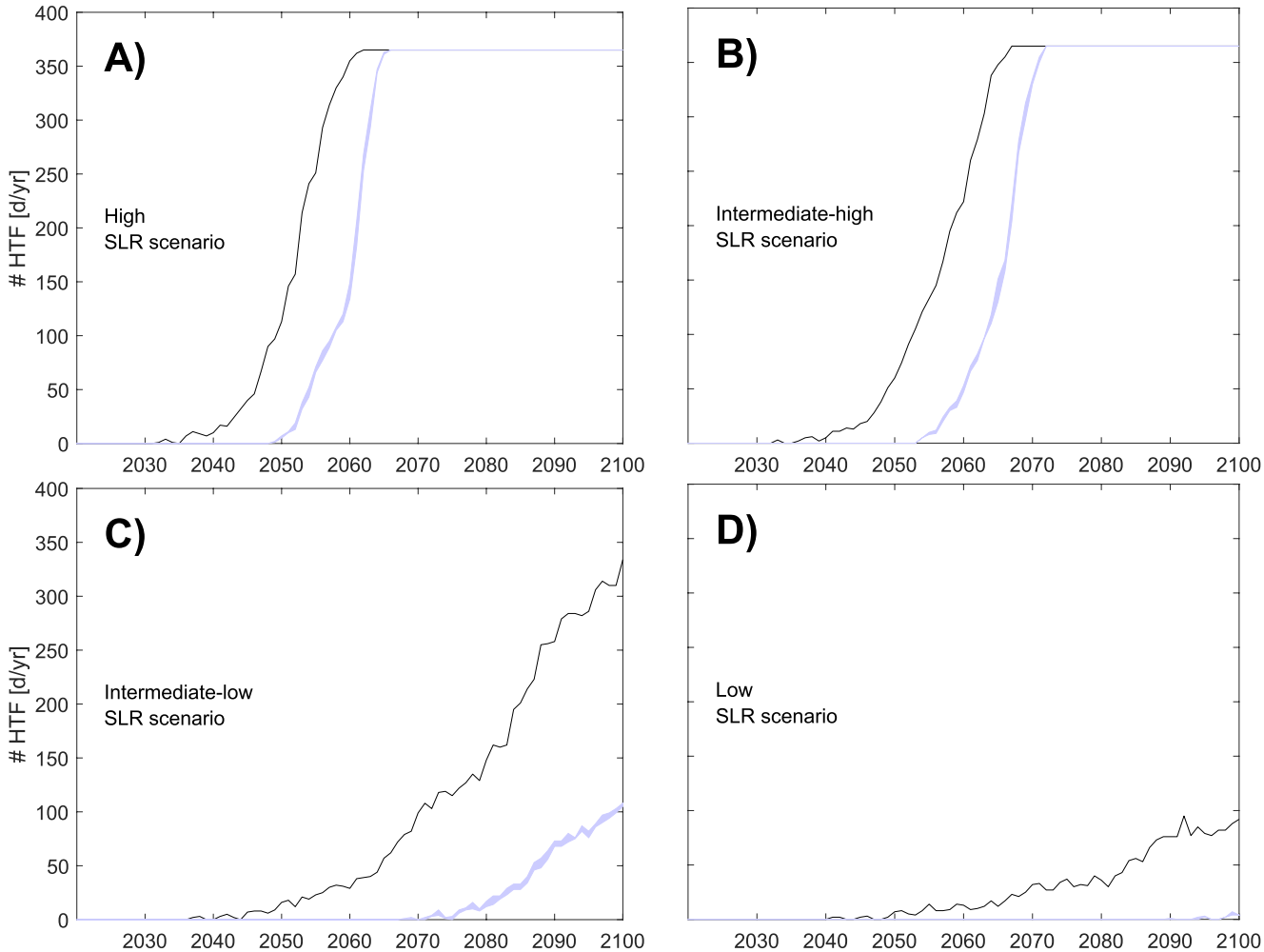

Figure 7. Projected yearly high-tide floods days at Miami under different tidal conditions and sea level rise (SLR) scenarios (tide-only floods). Black and blue coloring refers to modern and historical tidal conditions. Shaded area indicate the results related to the bounds of the inferred historical constituents. Panel (a): high SLR scenario; panel (b): intermediate-high SLR scenario; panel (c): intermediate-low SLR scenario; panel (d): low SLR scenario.

The transition to chronic flooding (>100 HTF per year) due to modern tides occurs almost simultaneously for the high and intermediate-high scenarios (2050 and 2053, respectively, see Table 2); similarly, the onset of permanent flooding (2062 and 2067) occurs within 5 years. A ∼30 years time lag between the onset of HTF and the transition to chronic flooding is estimated for the intermediate-low SLR scenarios for modern tides (Figure 7c); no chronic flooding caused only by tides is observed in the low SLR scenario for both modern and historical tides (Table 2). A return to historical tidal conditions would delay permanent flooding by 4 and 5 years compared to modern tides for high and intermediate high SLR scenarios, respectively. Historical tidal conditions produce chronic flooding ∼10 years later than modern tides under high and intermediate high scenarios. The delay is approximately 30 years under the intermediate-low SLR scenario. Results are statistically robust: the upper and lower bounds of the inferred constituents are similar both in terms of years and number of HTF days, and indicates that the uncertainty related to the constituent inference method does not significantly affect comparisons.

The analysis so far (Figures 7 and 8) only considers tidal oscillations and seasonal sea-level variability on top of projected MSLs (i.e., the tide-only scenario, see Section 2.3). This approach enables us to isolate the contribution of tides to HTF and provides useful metrics for quantifying the effects that tides and sea-level rise have on coastal flooding (Hague & Taylor, 2021). However, such analysis neglects other relevant forcing, such as inter-annual to decadal MSL variability, river discharge, storm surges, and non linear effects between forcing factors that can create deviations from predicted water levels (Jane et al., 2020). At gauge MRMS4, water levels differ from the predicted tide by a typical range of ±0.2 m, and this increases the number of possible pathways that HTF can

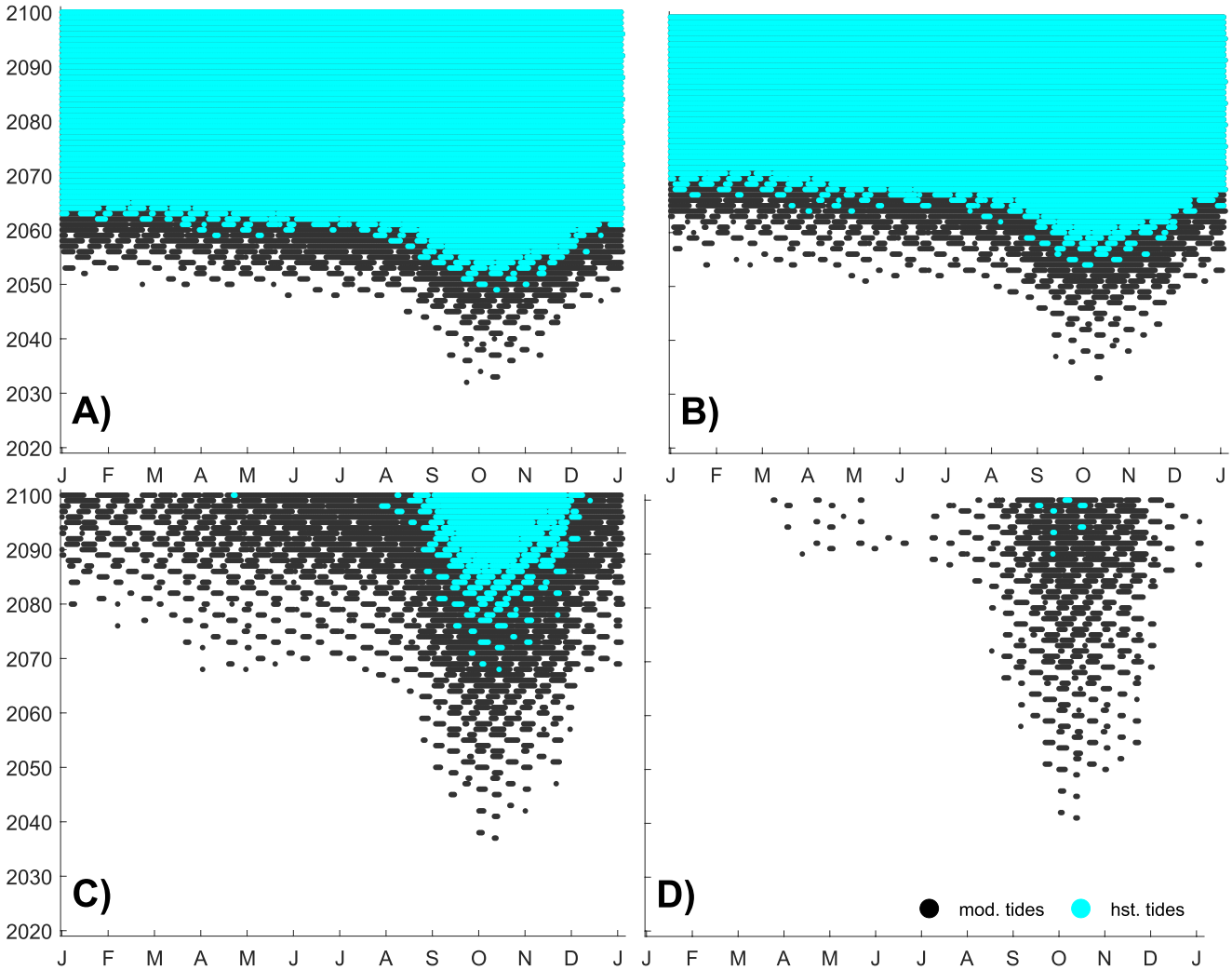

Figure 8. High-tide floods days in the 2022–2100 period at Miami (tide-only floods). Markers indicate days where the minor flood is exceeded at least once due to modern (2020) and historical (pre-1899) tidal conditions (black and cyan markers, respectively). Panel (a): high sea level rise (SLR); panel (b): intermediate-high SLR; panel (c): intermediate-low SLR; panel (d): low SLR.

occur (see Figure S2 in Supporting Information S1). Hence, the non-tidal residual was next included in projections (i.e., the TWL approach, Section 2.3; see Figure 9).

Results show that year-to-year variations in the time-series of total residuals tends to produce HTF earlier and more often in the first few decades that the datum is exceeded, but delays the transition to permanent flooding (compare the shaded areas with tide-only curves denoted by the solid lines). The onset of HTF in Figure 9 occurs earlier because tidal predictions are sometimes exceeded by the non-tidal residual, leading to more flooding events. At high levels of HTF occurrence, the non-tidal residual will suppress HW in some tides, leading to fewer datum exceedances than would occur with tides alone. For this reason, adding non-tidal motions to the HTF curve (Figure 9) tends to increase the time span it will take to transition from occasional to permanent high-tide flooding.

When the 20 cm lower M2020 datum is considered (Figures 9c and 9d), the number of occurrences of HTF in the 2000–2010 decade increases significantly, consistent to previous observations in the area (Hauer et al., 2021). When modern tides are considered, the first exceedance of the S2018 datum is computed in 2012 (see black crosses in the inset in panel a), while the exceedance of the M2020 datum was already observed in 2004, the first complete year in the data set. Our evaluation reveals that historical tides would significantly reduce the number of HTF occurrences: when the S2018 datum is considered, the total number of HTF days in the 2004–2020 period

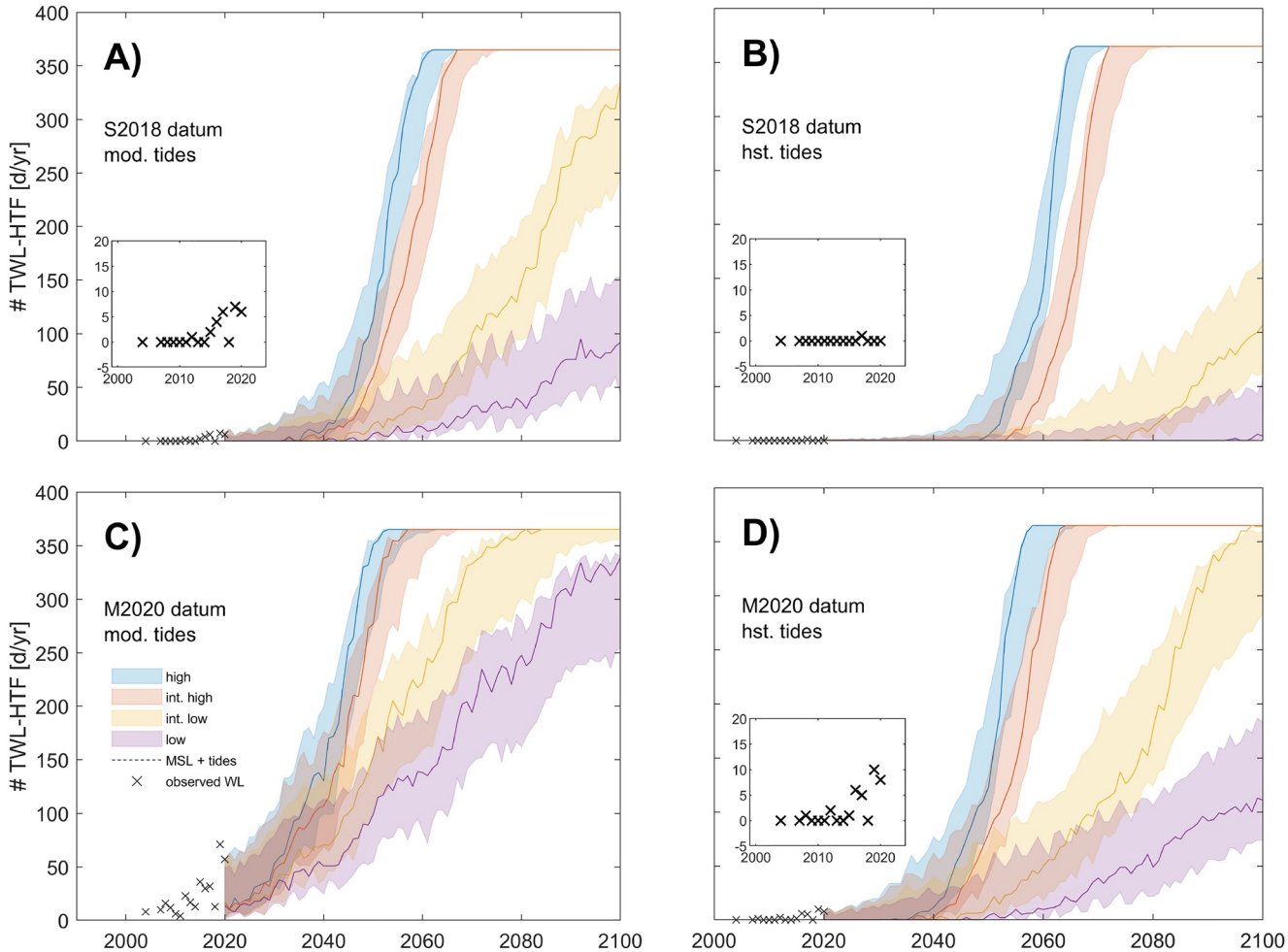

Figure 9. Number of yearly high-tide floods (HTF) days at Miami according to the total water level approach and different sea level rise scenarios. Panel (a): modern tidal conditions, S2018 datum; panel (b): historical tidal conditions, S2018 datum; panel (c): modern tidal conditions, M2020 datum; panel (d): historical tidal conditions, M2020 datum. Solid lines denote the tide-only HTF days (i.e., the curves in Figure 7), shaded areas denote the minimum and maximum estimates among the 15 series of total residuals employed. Results of panels (b and d) are related to the median values of the inferred historical constituents. Black crosses indicate the HTF days computed on the observed data (panels (a and c)), and according to the (Li et al., 2021) analysis.

Table 2
Statistics of the Differences Between 2022 and 2100 High-Tide Floods Days Driven by Modern and Historical Tidal Conditions at Miami (Tide-Only Floods)

SLR scenario	*Max ΔHTF [d/yr]*	*Year max ΔHTF*	*Tot ΔHTF[d]*	*Time span ΔHTF[yr]*	*Year chronic flooding*	*Year permanent flooding*
High	222–227	2058–2059	2804–2933	33	2058 (2050)	2066 (2062)
Int. high	220–228	2064	3096–3223	37	2064 (2053)	2072 (2067)
Int. low	226–229	2100	5814–5956	61	2099–2100 (2071)	– (–)
Low	95	2092	1995–2002	56	– (–)	– (–)

Note. The maximum difference in the number of HTF days is *max ΔHTF* and *year max ΔHTF* is the year in which this occurs. The number of years with differences in tide-only HTF days is *time ΔHTF*. Results between parenthesis denote the years of chronic and permanent flooding related to the modern tidal conditions. Cells with a range of values report the upper and lower bounds of results obtained from the inference method.

decreases from 26 to 1; using the lower M2020 datum, the HTFs are reduced by ∼90%, from 348 observed to only 33. These results show how the number of HTF depends critically on the datum used, with the lower M2020 datum leading to an earlier onset of flooding and a slightly different evolution over time. The comparatively later onset of future HTF flooding over the S2018 datum occurs at a larger SLR, due to the acceleration in MSL. The larger SLR produces a slight compression in the transition time from occasional to chronic flooding; this time difference, however, is slight, and not easily noticeable in Figure 9. The potential area flooded by exceeding the S2018 datum is substantially more (see Figure S5 in Supporting Information S1). Therefore, while exceedance of the S2018 datum occurs later in time, the potential impact is more severe.

The most important factor governing the transition time to chronic HTF and permanent HTF in Miami remains the SLR scenario, with changes to tides modulating the onset of chronic and permanent flooding (Figure 9). The low SLR scenario causes chronic flooding approximately 15 years after the high SLR scenario for modern tides (M2020 datum, Figure 9c). For historical tides, the comparable difference is ∼45 years after for historical tides (Figure 9c). Thus, as also found in Li et al. (2021), increased tides produce a larger difference in HTF trajectory when SLR is relatively small. The effects of SLR are cumulative, and the HTF numbers implied by different scenarios increasingly diverge with time. Because of the spread of possible HTF days, one cannot yet definitively discern which of the SLR trajectories most closely resembles measurements. Our results suggest that within 1–2 decades, when the scenarios clearly diverge, one should be able to assess which of our HTF projections most closely resembles measurements. However, our analysis of the rate of change of SLR within Biscayne Bay and at MRMS4 suggests that the region is most closely following the intermediate high or high SLR trajectory (Figure S3 in Supporting Information S1).

4. Discussion

The increase in the composite choking number by a factor of nearly 5 (Section 3.3) is an indicative summary measure that points to inlet modifications as a primary driver of altered tides and HTF events. Our results suggest that the ∼16.5 km^2 decrease in tidally influenced surface area within the Northern Biscayne Bay only marginally influences the choking number by ∼10% (see the repository in the Data Availability Statement). Additionally, changes are likely influenced by alterations to the depth and width of the inlet channels (Table S1 and Figures S6 and S7 in Supporting Information S1). Tidal attenuation may still be occurring at individual inlets; for example, tidal range reduces by 0.23 m between the seaward and landward side of Baker's Haulover inlet, in Northern Biscayne Bay. Because no inlet existed in 1900, even an attenuated tidal forcing through the inlet has likely impacted tides and HTF within Northern Biscayne Bay. The spatial pattern of tidal range changes caused by inlet creation, dredging and modification, and the combined effect of all changes, can only be assessed using analytic or numerical modeling approaches (Aretxabaleta et al., 2017, 2019; Wong & DiLorenzo, 1988). Such an analysis is beyond the scope of this effort, and is left for future research.

Another possible factor influencing tidal change is the marked gradient in tidal amplitudes that occurs along the eastern Florida coast, from 1.8 m at Fernandina (north-eastern Florida, see Figure S1 in Supporting Information S1) to 0.4 m at Key West in the southern end. At Biscayne Bay, modern coastal tidal range decreases by ∼0.28 m (from 0.9 to 0.62 m) from Haulover Inlet to Cape Florida, over a distance of 27 km. The dredging of new channels (Government Cut and Baker's Haulover Channel) in Northern Biscayne Bay may have effectively increased the tidal amplitude at the boundary of the bay, by providing access to Biscayne Bay to the larger northern tides. The primary access to Miami used to be from the South (see historical shipping channel, Figure 2), but is now at Government Cut. In fact, the tidal range change in the northern bay appears to be radiating southwards, causing tidal range increases at Cape Florida and other locations. Additionally, the increase in the average depth of Biscayne Bay may have altered tidal phase speeds and reflection effects, potentially increasing tidal amplitudes. A hydrodynamic model would be required to substantiate these observations (see e.g., Pelling et al., 2013), and it is possible that some frictional factors that we are unable to ascertain (such as changed bed morphology or altered sea-grass extent) are also influencing tidal amplitudes. The hardening of the coast-line and its influence on tidal reflection (Talke & Jay, 2020), wind driven circulation and water level setup, and interaction between multiple inlets (Aretxabaleta et al., 2019) may also be important for tides and non-tidal residuals.

The evolution of tidal properties within Biscayne Bay (particularly in the southern bay) and its detrimental influence on high-tide flood hazard may mean that extreme storm surge hazard has also increased over time, as also

observed in other heavily modified estuaries marked by a doubling in tidal range (e.g., Familkhalili & Talke, 2016; Talke et al., 2021). The last major hurricane to directly strike Miami, the West Indian Hurricane of September 1926, made landfall as a Category 3 hurricane with a sustained wind speed of 123 mph (almost 200 kmph), a low pressure reading of 931 mBar, and an estimated stormtide (tide + surge) of 2.4 m above sea-level. Because the Government Cut was only ~4.6 m deep in 1926, compared to 15 m deep today (Figure 6), it is likely that the storm surge wave was more choked (attenuated) than it would be today. A change in surge-wave attenuation through Government Cut is particularly likely given the inverse relationship between wave amplitude and the choking number and the relatively fast progression (small period T) of the 1926 storm. Both factors (large surge and fast progression) have been found to produce attenuation through other inlets (e.g., Orton et al., 2015). Moreover, tidal range was less in 1926 in Miami, leading to a smaller potential storm tide, if storm surge occurred at high tide. Indeed, tidal measurements in 1919 (the closest in time to 1926) suggest a tidal range of 0.42 m, approximately 0.24 m less than today. Both factors (decreases in surge and tidal magnitude) have been shown to cause lower magnitude of the 100 years flood height in retrospective simulations for the 1870s in another lagoonal estuary (Orton et al., 2020). While a hydrodynamic simulation would be required to prove the hypothesis that Miami has become more vulnerable to storm surge, the potentially large impact motivates further investigation. In any case, we can conclude, with confidence, that a storm tide occurring at high-water will produce a larger water level today than in 1900, due to the doubling of tidal range. Our case-study results may have implications for the coastal engineering and policy management of lagoonal systems. The US Army Corps of Engineers maintains and manages over 400 inlets in the United States, including many that are much deeper than they were historically (Dean & O'Brien, 1987). Tides in some lagoons also react to other geometric changes, land reclamation, and sea-level rise (e.g., Araújo et al., 2008; Donatelli et al., 2018; Passeri et al., 2016). Based on these considerations, it is likely that the high-tide flood hazard of other lagoons has also changed due to tidal evolution, in addition to the river estuary systems identified in Li et al. (2021). In some cases, as suggested by Orton et al. (2015); Orton et al. (2020), one may be able to reduce flood hazard by shallowing channels to be closer to historical norms.

A number of assumptions and approximations have been made in the analysis presented here, both in the inference-based constituent estimates, the evaluation of high-tide flooding, and the estimation of the choking number. Our composite choking number estimate neglects the Southern Biscayne Bay region; nonetheless, splitting the dynamics of Biscayne Bay into a northern and southern portion is consistent with previous studies (Dean & Taylor, 1973; Schneider, 1969). Because our inferential approach is under-constrained, we cannot infer the effect of possible trends in minor constituents such as K_2 or MK_3; however, trends in minor constituents are often undetectable, or of small magnitude compared to the major constituents (e.g., Woodworth, 2010). Hence, we neglected changes to the smaller constituents and assess our method compared with Li et al. (2021), which implicitly includes any changes to minor constituents in its approach. Moreover, when predicting tides through 2100, we assumed that no trend will affect future tidal constituent magnitudes. Our evaluation of the MRMS4 gauge and the Virginia Key gauge suggests that tidal properties near Miami have changed little over the past 30 years (Figure S8 in Supporting Information S1), supporting the assumption of stationary future tidal properties. Within the Southern Biscayne Bay Region, and at one Northern Biscayne Bay station, statistically significant trends in tidal properties are observed (Figure S8 in Supporting Information S1). However, these gauges are outside our focus area and are characterized both by different tidal ranges and likely different minor-flood datums. Negligible trends are also found in Miami Beach, and are consistent with Flick et al. (1999); Flick et al. (2003). However, future changes in the major tidal constituents cannot be ruled out, either due to increased SLR effects (Schindelegger et al., 2018) and/or further modifications to inlets geometry. We note that possible future tidal constituent changes in the Atlantic Ocean (1%–5% in Schindelegger et al., 2018) are small relative to the doubling of tidal range that occurred historically in Miami. The projection of (possibly small) future trends in tides is uncertain, and therefore is beyond the scope of this research and is left to future study.

The reason that our analysis yields reasonable, plausible insights into the effect of changing tides on flooding is that the signal-to-noise ratio is large. Though tidal range tabulations are based on short data series, past experience with similar hydrographic measurements (Helaire et al., 2019; Talke & Jay, 2017; Talke et al., 2021) suggests that they are accurate to within 0.02 or 0.03 m. A similar accuracy is observed in our historical inferences of M_2, based on tabulations of MTR (e.g., Figure 4). Because tidal range increased by 0.34 m at Miami, uncertainties in tidal properties are relatively small compared to the change signal, and our approach is able to discern the effects of tidal evolution. For locations with a much smaller magnitude change in tides, our approach may not be suitable. Similarly, experimentation suggested that Equation 1 is less accurate in diurnal systems (e.g.,

Gulf Coast) and less reliable in mixed semi-diurnal systems (such as the U.S. West Coast). Finally, our approach may require modifications in locations where river discharge significantly influences tidal properties (see e.g., Kukulka & Jay, 2003).

5. Conclusion

In this contribution, we develop a method to characterize the effects that evolving tides have on high-tide flooding when historical information of tidal change is limited. The method enables estimation of an ensemble of historical tidal constituents, given only estimates of historical tidal range plus modern constituents and constituent ratios (Sections 2.1 and 2.2). Results suggest that estimates of M_2 are statistically indistinguishable from direct harmonic estimates in the majority of tested cases, though the uncertainty in inferred constituents is higher due to the spread of values in each ensemble of estimates. Further, the estimates of M_2 based on MTR are able to capture both year-to-year variations and long-term trends in the M_2 constituent. The inference-based method of estimating tides is then applied to Miami, Florida, a major port city in which available tabulations suggest that tidal range has doubled. The cause of tidal changes is likely local anthropogenic development and land use changes that occurred primarily in the first half of the 20th century. Changes included the digging of two new channels through the barrier islands that protect Miami from the ocean (Government Cut and Baker's Haulover Inlet) and the removal of ∼16.5 square kilometers of northern Biscayne Bay from tidal influence. A scaling analysis suggests that the choking number has increased by a factor of five. This is consistent with the hypothesis that increased inlet cross-sectional area enabled increased tidal exchange, such that Biscayne Bay tides now closely resemble coastal tides. Moreover, because tides increase sharply in the northerly direction along the coast (Figure 6), the dredging of new channels enabled the larger northern tides to exert more influence on Biscayne Bay.

The influence of tidal change, and hence changing HTF evolution, is estimated using the method of Li et al. (2021), in which modern tides are removed from data and replaced by historical predictions. Results show that the doubling of tidal range in Miami has caused HTF to occur approximately a decade earlier than would have occurred in the historical tidal regime, and that change in tides in the high SLR scenario will produce almost 3000 more tide-only HTF days over the 2033–2065 period. Potential flood mitigation measures could include reversing bathymetry changes and restricting the open ocean exchange of water to reduce tidal ranges to historical levels, reducing in turn potential effects and damage from both present and future high-tide flooding. The observed doubling of tidal range in Miami and its influence on high-tide flooding suggests that other back-barrier bays and lagoons should be evaluated for the effects of anthropogenic change. The case study presented here therefore provides a template for ascertaining the causes and consequences of tidal evolution in lagoonal-type estuaries, and characterizing their impact.

Data Availability Statement

The U-Tide routine used to perform the harmonic analysis is available for download at: https://www.mathworks.com/matlabcentral/fileexchange/46523-utide-unified-tidal-analysis-and-prediction-functions. National Oceanic and Atmospheric Administration time-series are available for download at: https://tidesandcurrents.noaa.gov/. Miami Beach data from 1931 to 1974 are available in GESLA-3 (https://gesla787883612.wordpress.com/). SFWMD time-series are available for download at: https://www.sfwmd.gov/science-data/levels. Modern bathymetry data of the Biscayne Bay are available for download at: https://www.ncei.noaa.gov/access/metadata/landing-page/bin/iso?id=gov.noaa.ngdc.mgg.dem:biscayne_bay_S200_2018. Historical documents with tidal range measurements, geo-referenced tif files of the digitized Coast Survey charts (Section 2.4), and water level series projected through 2100 at MRMS4 location (Section 2.3) are available for download at the following repository: https://doi.org/10.5281/zenodo.6551549.

Acknowledgments
This work was supported by the National Science Foundation, project numbers 2013280 (F. De Leo, S. A. Talke), 1455350 (S. A. Talke), 1854896 (T. Wahl), 1855037 (P. M. Orton). The authors acknowledge the kind support and the help provided by Sida Li, and the students (Sofia S. Barale, Alexandra Kuesel, Sophia Rosenburg and Joshua S. Rowe) that helped digitize the historical Biscayne Bay map. Open Access Funding provided by Universita degli Studi di Genova within the CRUI-CARE Agreement.

References

Araújo, I., Dias, J., & Pugh, D. (2008). Model simulations of tidal changes in a coastal lagoon, the Ria de Aveiro (Portugal). *Continental Shelf Research*, *28*(8), 1010–1025. https://doi.org/10.1016/j.csr.2008.02.001

Aretxabaleta, A. L., Ganju, N. K., Butman, B., & Signell, R. P. (2017). Observations and a linear model of water level in an interconnected inlet-bay system. *Journal of Geophysical Research: Oceans*, *122*(4), 2760–2780. https://doi.org/10.1002/2016jc012318

Aretxabaleta, A. L., Ganju, N. K., Defne, Z., & Signell, R. P. (2019). Spatial distribution of water level impacting back-barrier bays. *Natural Hazards and Earth System Sciences*, *19*(8), 1823–1838. https://doi.org/10.5194/nhess-19-1823-2019

Cantillo, A. Y., Pikula, L., Hale, K. K., Collins, E. V., & Caballero, R. (2000). *Biscayne Bay environmental history and annotated bibliography (Tech. Rep. No. 145)*. U.S.: National Centers for Coastal Ocean Science (U.S.).
Cartwright, D., & Tayler, R. (1971). New computations of the tide-generating potential. *Geophysical Journal International*, *23*(1), 45–73. https://doi.org/10.1111/j.1365-246x.1971.tb01803.x
CGS. (1952). Manual of harmonic constant reduction [Computer software manual]. *United States Government Printing Office*
Chant, R. J., Sommerfield, C. K., & Talke, S. A. (2018). Impact of channel deepening on tidal and gravitational circulation in a highly engineered estuarine basin. *Estuaries and Coasts*, *41*(6), 1587–1600. https://doi.org/10.1007/s12237-018-0379-6
Chernetsky, A. S., Schuttelaars, H. M., & Talke, S. A. (2010). The effect of tidal asymmetry and temporal settling lag on sediment trapping in tidal estuaries. *Ocean Dynamics*, *60*(5), 1219–1241. https://doi.org/10.1007/s10236-010-0329-8
Codiga, D. L. (2011). *Unified tidal analysis and prediction using the UTide Matlab functions (Tech. Rep. No. 01)*. Graduate School of Oceanography, University of Rhode Island.
Dean, R., & O'Brien, M. (1987). *Florida's East Coast inlets shoreline effects and recommended action Tech. Rep. No. 87/017*. U.S.: University of Florida, Coastal and Oceanographic Engineering Department.
Dean, R., & Taylor, R. (1973). Numerical modeling of constituent transport in bay systems. *Coastal Engineering*, *1972*(13), 2227–2249. https://doi.org/10.9753/icce.v13.123
Department of the Interior, U. S. (2002). National register of historic places. (continuation sheet). Retrieved from https://npgallery.nps.gov/GetAsset/9074c621-a52c-432d-9968-60365e1ddcbf
Devlin, A., Jay, D., Talke, S., & Zaron, E. (2014). Tidal trends associated with anomalous sea level rise in the Western Pacific Ocean. *Ocean Dynamics*, *64*(8), 1093–1120. https://doi.org/10.1007/s10236-014-0741-6
DiLorenzo, J. L., Huang, P., Thatcher, M. L., & Najarian, T. O. (1993). Dredging impacts on Delaware estuary tides. In *Estuarine and coastal modeling* (pp. 86–104).
Domingues, R., Goni, G., Baringer, M., & Volkov, D. (2018). What caused the accelerated sea level changes along the US East Coast during 2010–2015? *Geophysical Research Letters*, *45*(24), 13–367. https://doi.org/10.1029/2018gl081183
Donatelli, C., Ganju, N. K., Zhang, X., Fagherazzi, S., & Leonardi, N. (2018). Salt marsh loss affects tides and the sediment budget in shallow bays. *Journal of Geophysical Research: Earth Surface*, *123*(10), 2647–2662. https://doi.org/10.1029/2018jf004617
Du, J., Shen, J., Zhang, Y. J., Ye, F., Liu, Z., Wang, Z., et al. (2018). Tidal response to sea-level rise in different types of estuaries: The Importance of Length, Bathymetry, and Geometry. *Geophysical Research Letters*, *45*(1), 227–235. https://doi.org/10.1002/2017gl075963
Familkhalili, R., & Talke, S. A. (2016). The effect of channel deepening on tides and storm surge: A case study of Wilmington, NC. *Geophysical Research Letters*, *43*(17), 9138–9147. https://doi.org/10.1002/2016gl069494
Fiaschi, S., & Wdowinski, S. (2020). Local land subsidence in Miami Beach (FL) and Norfolk (VA) and its contribution to flooding hazard in coastal communities along the US Atlantic Coast. *Ocean & Coastal Management*, *187*, 105078. https://doi.org/10.1016/j.ocecoaman.2019.105078
Flick, R. E., Murray, J. F., & Ewing, L. C. (1999). *Trends in US tidal datum statistics and tide range: A data report atlas*. Center for Coastal Studies, Scripps Institution of Oceanography.
Flick, R. E., Murray, J. F., & Ewing, L. C. (2003). Trends in United States tidal datum statistics and tide range. *Journal of Waterway, Port, Coastal, and Ocean Engineering*, *129*(4), 155–164. https://doi.org/10.1061/(asce)0733-950x(2003)129:4(155)
Foreman, M. G. G. (1979). *Manual for tidal heights analysis and prediction*. Institute of Ocean Sciences.
Foreman, M. G. G., & Henry, R. F. (1989). The harmonic analysis of tidal model time series. *Advances in Water Resources*, *12*(3), 109–120. https://doi.org/10.1016/0309-1708(89)90017-1
Hague, B. S., & Taylor, A. J. (2021). Tide-only inundation: A metric to quantify the contribution of tides to coastal inundation under sea-level rise. *Natural Hazards*, *107*(1), 675–695. https://doi.org/10.1007/s11069-021-04600-4
Haigh, I. D., Eliot, M., & Pattiaratchi, C. (2011). Global influences of the 18.61 year nodal cycle and 8.85 year cycle of lunar perigee on high tidal levels. *Journal of Geophysical Research*, *116*(C6), C06025. https://doi.org/10.1029/2010jc006645
Haigh, I. D., Marcos, M., Talke, S. A., Woodworth, P. L., Hunter, J. R., Haugh, B. S., et al. (2021). GESLA version 3: A major update to the global higher-frequency sea-level dataset.
Hall, G. F., Hill, D. F., Horton, B. P., Engelhart, S. E., & Peltier, W. (2013). A high-resolution study of tides in the Delaware Bay: Past conditions and future scenarios. *Geophysical Research Letters*, *40*(2), 338–342. https://doi.org/10.1029/2012gl054675
Hauer, M., Mueller, V., Sheriff, G., & Zhong, Q. (2021). More than a nuisance: Measuring how Sea Level rise delays commuters in Miami, FL. *Environmental Research Letters*, *16*(6), 064041. https://doi.org/10.1088/1748-9326/abfd5c
Helaire, L. T., Talke, S. A., Jay, D. A., & Mahedy, D. (2019). Historical changes in lower Columbia River and Estuary floods: A numerical study. *Journal of Geophysical Research: Oceans*, *124*(11), 7926–7946. https://doi.org/10.1029/2019jc015055
Hill, A. (1994). Fortnightly tides in a lagoon with variable choking. Estuarine. *Coastal and Shelf Science*, *38*(4), 423–434. https://doi.org/10.1006/ecss.1994.1029
Holleman, R. C., & Stacey, M. T. (2014). Coupling of sea level rise, tidal amplification, and inundation. *Journal of Physical Oceanography*, *44*(5), 1439–1455. https://doi.org/10.1175/jpo-d-13-0214.1
H. R. (1909). Letter by spalding, Geo R. In *Proceedings of the 61st congress, 1st session* (pp. 1–5). Government Printing Office.
Jane, R., Cadavid, L., Obeysekera, J., & Wahl, T. (2020). Multivariate statistical modelling of the drivers of compound flood events in south Florida. *Natural Hazards and Earth System Sciences*, *20*(10), 2681–2699. https://doi.org/10.5194/nhess-20-2681-2020
Jay, D. A. (2009). Evolution of tidal amplitudes in the eastern Pacific Ocean. *Geophysical Research Letters*, *36*(4), L04603. https://doi.org/10.1029/2008gl036185
Jay, D. A., Leffler, K., & Degens, S. (2011). Long-term evolution of Columbia River tides. *Journal of Waterway, Port, Coastal, and Ocean Engineering*, *137*(4), 182–191. https://doi.org/10.1061/(asce)ww.1943-5460.0000082
Kukulka, T., & Jay, D. A. (2003). Impacts of Columbia River discharge on salmonid habitat: 1. A nonstationary fluvial tide model. *Journal of Geophysical Research*, *108*(C9), 3293. https://doi.org/10.1029/2002jc001382
Lee, S. B., Li, M., & Zhang, F. (2017). Impact of sea level rise on tidal range in Chesapeake and Delaware Bays. *Journal of Geophysical Research: Oceans*, *122*(5), 3917–3938. https://doi.org/10.1002/2016jc012597
Li, S., Wahl, T., Talke, S. A., Jay, D. A., Orton, P. M., Liang, X., et al. (2021). Evolving tides aggravate nuisance flooding along the US coastline. *Science Advances*, *7*(10), eabe2412. https://doi.org/10.1126/sciadv.abe2412
Manning, T. G. (1988). *US coast survey vs. naval hydrographic office: A 19th-century rivalry in science and politics*. University of Alabama Press.
McAlpine, S. A., & Porter, J. R. (2018). Estimating recent local impacts of sea-level rise on current real-estate losses: A housing market case study in Miami-Dade, Florida. *Population Research and Policy Review*, *37*(6), 871–895. https://doi.org/10.1007/s11113-018-9473-5

Moftakhari, H. R., AghaKouchak, A., Sanders, B. F., Allaire, M., & Matthew, R. A. (2018). What is nuisance flooding? Defining and monitoring an emerging challenge. *Water Resources Research*, *54*(7), 4218–4227. https://doi.org/10.1029/2018wr022828

Moftakhari, H. R., AghaKouchak, A., Sanders, B. F., Feldman, D. L., Sweet, W., Matthew, R. A., & Luke, A. (2015). Increased nuisance flooding along the coasts of the United States due to sea level rise: Past and future. *Geophysical Research Letters*, *42*(22), 9846–9852. https://doi.org/10.1002/2015gl066072

Moftakhari, H. R., AghaKouchak, A., Sanders, B. F., & Matthew, R. A. (2017). Cumulative hazard: The case of nuisance flooding. *Earth's Future*, *5*(2), 214–223. https://doi.org/10.1002/2016ef000494

Moftakhari, H. R., Jay, D. A., Talke, S. A., Kukulka, T., & Bromirski, P. D. (2013). A novel approach to flow estimation in tidal rivers. *Water Resources Research*, *49*(8), 4817–4832. https://doi.org/10.1002/wrcr.20363

Molinaroli, E., Guerzoni, S., & Suman, D. (2019). Do the adaptations of Venice and Miami to sea level rise offer lessons for other vulnerable coastal cities? *Environmental Management*, *64*(4), 391–415. https://doi.org/10.1007/s00267-019-01198-z

Moore, F. C., & Obradovich, N. (2020). Using remarkability to define coastal flooding thresholds. *Nature Communications*, *11*(1), 1–8. https://doi.org/10.1038/s41467-019-13935-3

Neumann, J. E., Emanuel, K., Ravela, S., Ludwig, L., Kirshen, P., Bosma, K., & Martinich, J. (2015). Joint effects of storm surge and sea-level rise on US Coasts: New economic estimates of impacts, adaptation, and benefits of mitigation policy. *Climatic Change*, *129*(1), 337–349. https://doi.org/10.1007/s10584-014-1304-z

Orton, P. M., Sanderson, E. W., Talke, S. A., Giampieri, M., & MacManus, K. (2020). Storm tide amplification and habitat changes due to urbanization of a lagoonal estuary. *Natural Hazards and Earth System Sciences*, *20*(9), 2415–2432. https://doi.org/10.5194/nhess-20-2415-2020

Orton, P. M., Talke, S. A., Jay, D. A., Yin, L., Blumberg, A. F., Georgas, N., et al. (2015). Channel shallowing as mitigation of coastal flooding. *Journal of Marine Science and Engineering*, *3*(3), 654–673. https://doi.org/10.3390/jmse3030654

Parker, B. B. (2007). *Tidal analysis and prediction*. NOAA, NOS Center for Operational Oceanographic Products and Services.

Passeri, D. L., Hagen, S. C., Plant, N. G., Bilskie, M. V., Medeiros, S. C., & Alizad, K. (2016). Tidal hydrodynamics under future sea level rise and coastal morphology in the Northern Gulf of Mexico. *Earth's Future*, *4*(5), 159–176. https://doi.org/10.1002/2015ef000332

Pawlowicz, R., Beardsley, B., & Lentz, S. (2002). Classical tidal harmonic analysis including error estimates in MATLAB using T_TIDE. *Computers & Geosciences*, *28*(8), 929–937. https://doi.org/10.1016/s0098-3004(02)00013-4

Pelling, H., Uehara, K., & Green, J. M. (2013). The impact of rapid coastline changes and sea level rise on the tides in the Bohai Sea, China. *Journal of Geophysical Research: Oceans*, *118*(7), 3462–3472. https://doi.org/10.1002/jgrc.20258

Ralston, D. K., Talke, S. A., Geyer, W. R., Al-Zubaidi, H. A., & Sommerfield, C. K. (2019). Bigger tides, less flooding: Effects of dredging on barotropic dynamics in a highly modified estuary. *Journal of Geophysical Research: Oceans*, *124*(1), 196–211. https://doi.org/10.1029/2018jc014313

Ray, R. D. (2006). Secular changes of the M2 tide in the Gulf of Maine. *Continental Shelf Research*, *26*(3), 422–427. https://doi.org/10.1016/j.csr.2005.12.005

Ray, R. D. (2009). Secular changes in the solar semidiurnal tide of the Western North Atlantic Ocean. *Geophysical Research Letters*, *36*(19), L19601. https://doi.org/10.1029/2009gl040217

Ray, R. D., & Foster, G. (2016). Future nuisance flooding at Boston caused by astronomical tides alone. *Earth's Future*, *4*(12), 578–587. https://doi.org/10.1002/2016ef000423

Ray, R. D., & Talke, S. A. (2019). Nineteenth-century tides in the Gulf of Maine and implications for secular trends. *Journal of Geophysical Research: Oceans*, *124*(10), 7046–7067. https://doi.org/10.1029/2019jc015277

Ross, A. C., Najjar, R. G., Li, M., Lee, S. B., Zhang, F., & Liu, W. (2017). Fingerprints of sea level rise on changing tides in the Chesapeake and Delaware Bays. *Journal of Geophysical Research: Oceans*, *122*(10), 8102–8125. https://doi.org/10.1002/2017jc012887

Schindelegger, M., Green, J., Wilmes, S.-B., & Haigh, I. D. (2018). Can we model the effect of observed sea level rise on tides? *Journal of Geophysical Research: Oceans*, *123*(7), 4593–4609. https://doi.org/10.1029/2018jc013959

Schneider, J. J. (1969). *Tidal relations in the south Biscayne bay area, dade county, Florida*. GEOL SURV OPEN-FILE REPORT. JAN 1969. 16 P, 6 FIG, 1 TAB.

Stigebrandt, A. (1980). Some aspects of tidal interaction with fjord constrictions. *Estuarine and Coastal Marine Science*, *11*(2), 151–166. https://doi.org/10.1016/s0302-3524(80)80038-7

Sweet, W. V., Dusek, G., Obeysekera, J., & Marra, J. J. (2018). *Patterns and projections of high tide flooding along the us coastline using a common impact threshold (Tech. Rep.)*. NOAA, NOS Center for Operational Oceanographic Products and Services.

Sweet, W. V., Kopp, R. E., Weaver, C. P., Obeysekera, J., Horton, R. M., Thieler, E. R., & Zervas, C. (2022). *Global and regional sea level rise scenarios for the United States (Tech. Rep. No. 01)*. NOAA.

Sweet, W. V., & Marra, J. (2015). *State of us "nuisance" tidal flooding*. NOAA Report.

Sweet, W. V., & Park, J. (2014). From the extreme to the mean: Acceleration and tipping points of coastal inundation from sea level rise. *Earth's Future*, *2*(12), 579–600. https://doi.org/10.1002/2014ef000272

Taherkhani, M., Vitousek, S., Barnard, P. L., Frazer, N., Anderson, T. R., & Fletcher, C. H. (2020). Sea-level rise exponentially increases coastal flood frequency. *Scientific Reports*, *10*(1), 1–17. https://doi.org/10.1038/s41598-020-62188-4

Talke, S. A., Familkhalili, R., & Jay, D. A. (2021). The influence of channel deepening on tides, river discharge effects, and storm surge. *Journal of Geophysical Research: Oceans*, *126*(5), e2020JC016328. https://doi.org/10.1029/2020jc016328

Talke, S. A., & Jay, D. A. (2013). Nineteenth century North American and Pacific tidal data: Lost or just forgotten? *Journal of Coastal Research*, *29*(6a), 118–127. https://doi.org/10.2112/jcoastres-d-12-00181.1

Talke, S. A., & Jay, D. A. (2017). *Archival water-level measurements: Recovering historical data to help design for the future*. Civil and Environmental Engineering Faculty Publications and Presentations. 412.

Talke, S. A., & Jay, D. A. (2020). Changing tides: The role of natural and anthropogenic factors. *Annual Review of Marine Science*, *12*(1), 121–151. https://doi.org/10.1146/annurev-marine-010419-010727

Talke, S. A., Kemp, A., & Woodruff, J. (2018). Relative sea level, tides, and extreme water levels in Boston Harbor from 1825 to 2018. *Journal of Geophysical Research: Oceans*, *123*(6), 3895–3914. https://doi.org/10.1029/2017jc013645

Talke, S. A., Mahedy, A., Jay, D. A., Lau, P., Hilley, C., & Hudson, A. (2020). Sea level, tidal, and river flow trends in the lower Columbia River Estuary, 1853–present. *Journal of Geophysical Research: Oceans*, *125*(3), e2019JC015656. https://doi.org/10.1029/2019jc015656

Talke, S. A., Orton, P., & Jay, D. A. (2014). Increasing storm tides in New York harbor, 1844–2013. *Geophysical Research Letters*, *41*(9), 3149–3155. https://doi.org/10.1002/2014gl059574

Thompson, P. R., Widlansky, M. J., Hamlington, B. D., Merrifield, M. A., Marra, J. J., Mitchum, G. T., & Sweet, W. (2021). Rapid increases and extreme months in projections of United States high-tide flooding. *Nature Climate Change*, *11*, 1–7. https://doi.org/10.1038/s41558-021-01077-8

USCP. (1900). *United States coast pilot: Atlantic coast. from chesapeake bay entrance to key west (No. pt. 7)*. U.S. Government Printing Office. Retrieved from https://books.google.it/books?id=8M07AQAAMAAJ

Valle-Levinson, A., Dutton, A., & Martin, J. B. (2017). Spatial and temporal variability of sea level rise hot spots over the eastern United States. *Geophysical Research Letters*, *44*(15), 7876–7882. https://doi.org/10.1002/2017gl073926

Wdowinski, S., Bray, R., Kirtman, B. P., & Wu, Z. (2016). Increasing flooding hazard in coastal communities due to rising sea level: Case study of Miami Beach, Florida. *Ocean & Coastal Management*, *126*, 1–8. https://doi.org/10.1016/j.ocecoaman.2016.03.002

Weiss, J. L., Overpeck, J. T., & Strauss, B. (2011). Implications of recent sea level rise science for low-elevation areas in coastal cities of the conterminous USA. *Climatic Change*, *105*(3), 635–645. https://doi.org/10.1007/s10584-011-0024-x

Winterwerp, J. C., & Wang, Z. B. (2013). Man-induced regime shifts in small estuaries—I: Theory. *Ocean Dynamics*, *63*(11–12), 1279–1292. https://doi.org/10.1007/s10236-013-0662-9

Wong, K.-C., & DiLorenzo, J. (1988). The response of Delaware's inland bays to ocean forcing. *Journal of Geophysical Research*, *93*(C10), 12525–12535. https://doi.org/10.1029/jc093ic10p12525

Woodworth, P. (2010). A survey of recent changes in the main components of the ocean tide. *Continental Shelf Research*, *30*(15), 1680–1691. https://doi.org/10.1016/j.csr.2010.07.002

Zaron, E. D., & Jay, D. A. (2014). An analysis of secular change in tides at open-ocean sites in the Pacific. *Journal of Physical Oceanography*, *44*(7), 1704–1726. https://doi.org/10.1175/jpo-d-13-0266.1